Françoise Chalot-Prat · Anne-Marie Boullier

Metasomatism in the subcontinental mantle beneath the Eastern Carpathians (Romania): new evidence from trace element geochemistry

Abstract A wide range of trace elements have been analysed in mantle xenoliths (whole rocks, clinopyroxene and amphibole separates) from alkaline lavas in the Eastern Carpathians (Romania), in order to understand the process of metasomatism in the subcontinental mantle of the Carpatho-Pannonian region. The xenoliths include spinel lherzolites, harzburgites and websterites, clinopyroxenites, amphibole veins and amphibole clinopyroxenites. Textures vary from porphyroclastic to granoblastic, or equigranular. Grain size increases with increasing equilibrium temperature of mineralogical assemblages and results from grain boundary migration. In peridotites, interstitial clinopyroxenes (cpx) and amphiboles resulted from impregnation and metasomatism of harzburgites or cpx-poor lherzolites by small quantities of a melt I with a melilitite composition. Clinopyroxenites, amphibole veins and amphibole clinopyroxenites are also formed by metasomatism as a result of percolation through fracture systems of large quantities of a melt II with a melanephelinite composition. These metasomatic events are marked by whole-rock enrichments, relative to the primitive mantle (PM), in Rb, Th and U associated in some granoblastic lherzolites and in clinopyroxene and amphibole veins with enrichments in LREE, Ta and Nb. Correlations between major element whole-rock contents in peridotites demonstrate that the formation of interstitial amphibole and clinopyroxene induced only a slight but variable increase of the Ca/Al ratio without apparent modifications of the initial mantle composition. Metasomatism is also traced by enrichments in the most incompatible elements and the LREE. The Ta, Nb, MREE and HREE contents remained unchanged and confirm the depleted state of the initial but heterogeneous mantle. Major and trace element signature of clinopyroxene suggests that amphibole clinopyroxenites and some granoblastic lherzolites have been metasomatized successively by melts I and II. Both melts I and II were Ca-rich and Si-poor, somewhat alkaline (Na > K). Melt I differed from melt II in having higher Mg and Cr contents offset by lower Ti, Al, Fe and K contents. Both were highly enriched in all incompatible trace elements relative to primitive mantle, showing positive anomalies in Rb, Ba, Th, Sr and Zr. They contrasted by their Ta, Nb and LREE contents, lower in melt I than in melt II. Melts I and II originate during a two-stage melting event from the same source at high pressure and under increasing temperature. The source assemblage could be that of a metasomatized carbonated mantle but was more likely that of an eclogite of crustal affinity. Genetic relationships between calc-alkaline and alkaline lavas from Eastern Carpathians and these melts are thought to be only indirect, the former originating from partial melting of mantle sources respectively metasomatized by the melts I and II.

F. Chalot-Prat (✉)
University Henri Poincaré of Nancy, BP 239,
F-54506 Vandoeuvre-lès-Nancy, France
E-Mail: chalot@cnrs.crpg-nancy.fr
Fax: 33 3 83 51 17 98

A.M. Boullier[1]
CNRS-CRPG, BP 20, F-54501 Vandoeuvre-lès-Nancy, France

[1] *Present address*: LGIT-CNRS, IRIGM, BP 53X, F-38041 Grenoble
cedex, France

Editorial responsibility: J. Touret

Introduction

Petrographical, chemical and Sr-Nd isotopic studies have been performed on mantle xenoliths (Vaselli et al. 1995) entrained by alkaline lavas dated at 2.5 to 0.7 Ma (Downes et al. 1995) in the Persani Mountains (eastern Transylvanian Basin, Romania). This alkaline volcanism occurred at the same time as the younger stages of calc-alkaline volcanism of the Harghita area (Pécskay et al. 1995; Seghedi et al. 1995) at only about 25 km west of the East Carpathian arc. Vaselli et al. (1995) have shown that the shallow lithospheric depleted mantle was affected by a metasomatic event as indicated by the

existence of disseminated Ti-, K- and LREE-poor pargasite in peridotites on one hand, and concentration of Ti-, K- and LREE-rich Mg-hastingsite in amphibole pyroxenites and veins or, Ti- and LREE-rich but Cr-poor clinopyroxenes in clinopyroxenites on the other hand. The compositional difference between interstitial and vein amphiboles was assumed to be due to a sub-solidus re-equilibration of interstitial amphiboles with host-peridotite minerals after the metasomatic event, whereas veins were assumed mainly to result from a magmatic crystallization from an alkaline basic magma in opened fractures.

The present investigation was undertaken in order to characterize the trace element signature of these metasomatized mantle rocks, their clinopyroxenes and amphiboles, using the same samples investigated by Vaselli et al. (1995). This approach led us: (1) to investigate closely the fabric of these rocks and to correlate the changes in the trace element composition of an initially residual mantle with the appearance of metasomatic minerals through two successive percolation events, interpretation which diverges from that given by Vaselli et al. (1995); (2) to estimate the major and trace element composition of the two contaminant melts and to deduce their genetic relationships.

Petrography

Textures of the Persani Mts xenoliths (Table 1) have been classified using the nomenclature of Harte (1976) and Mercier (1985). Three main textural types have been distinguished: porphyroclastic, granoblastic and granuloblastic textures. Except for some differences in terminology, the textural determinations proposed here are similar to those of Vaselli et al. (1995) using the classification of Mercier and Nicolas (1975).

The porphyroclastic rocks (i.e. Bgt 6, Fig. 1; most of the BG and Bgt samples, Fig. 2) show deformed centimetric orthopyroxene crystals. Olivine crystals have a bimodal grain size with a heteroblastic texture (Mercier 1985), the smallest crystals resulting from dynamic recrystallization of the largest. The average size of the recrystallized crystals is homogeneous in some xenoliths (i.e. Bgt 6, Fig. 1; BG01, Bgt07, Bgt19..., Fig. 2) but varies in others (i.e. BG09 and BG16, Fig. 2). Olivine-olivine grain boundaries are straight or slightly curved. Although spinel may be observed in small grains around orthopyroxene i.e. Bgt06, Fig. 1, there is no close spatial association of clinopyroxene (plus spinel) with orthopyroxene as described by Mercier and Nicolas (1975).

Granoblastic samples (i.e. Bgt18 and BG18, Fig. 1; BG02, BG03, BG18, Bgt03, Bgt18 and Bgt22, Fig. 2) show large orthopyroxene and olivine crystals. Most of the olivine crystals are undeformed and have straight or curved grain boundaries but a few large crystals, however, display straight subgrain boundaries.
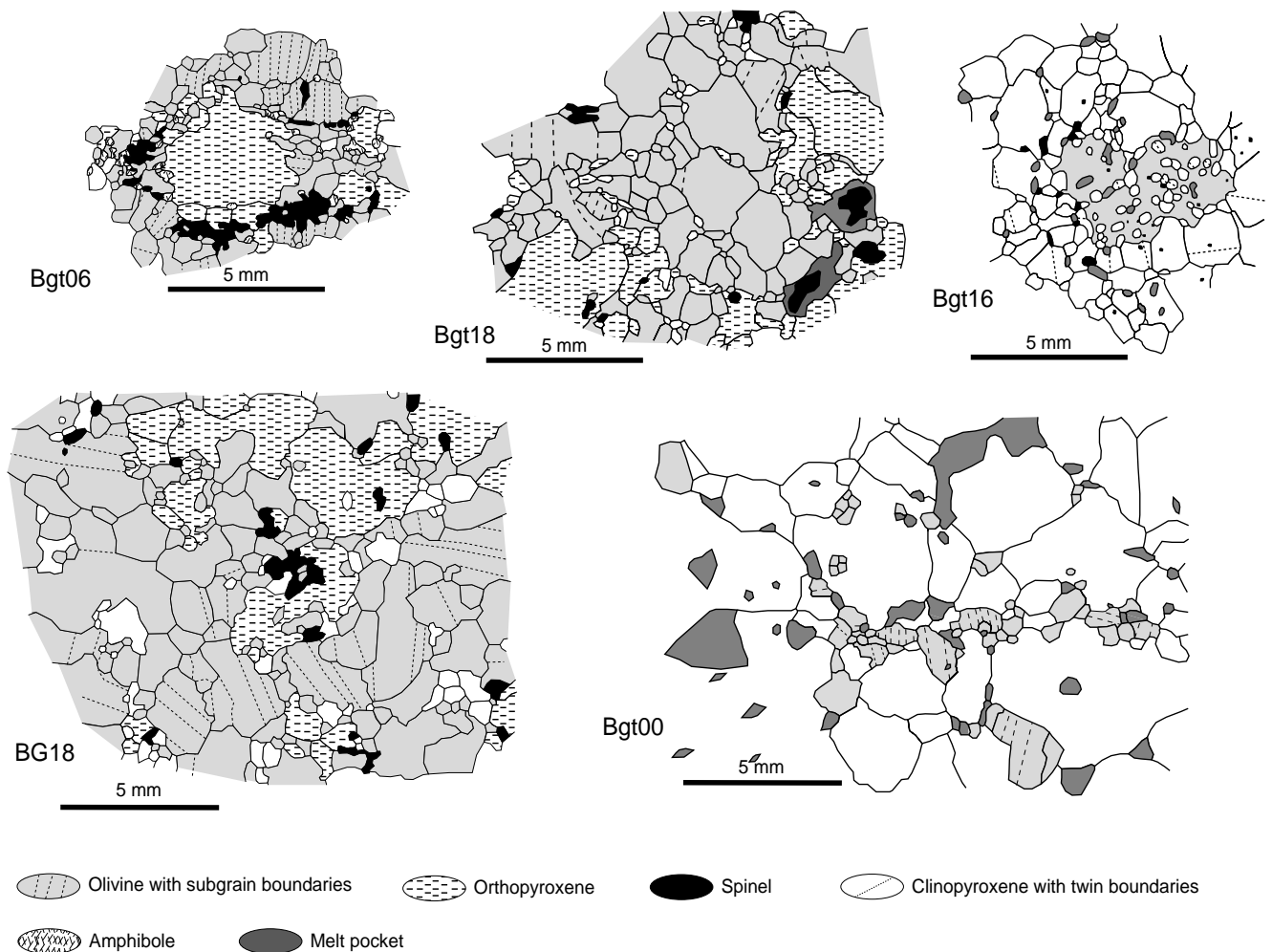
In the granuloblastic texture (BC09) small blebs of spinel are included in subequant and undeformed olivine crystals. Orthopyroxene and clinopyroxene also have regular and rounded shapes, the average grain size of the rock being unimodal and small relative to the other textural types. These observations suggest that minerals have reached textural equilibrium by extensive recrystallization.

Clinopyroxene crystals are undeformed and irregular in shape. In porphyroclastic lherzolites, the clinopyroxene crystals are small (< 500 μm) and relatively heterogeneous in size, interstitial, isolated and/or located at triple junctions or along grain boundaries (i.e. Bgt18, Fig. 1). In granoblastic lherzolites, their size is larger and relatively homogeneous (1 mm in BG18, Fig. 1). Regardless of their habit, they do not show a systematic relationship with any other mineral phase, although they locally surround some spinel grains.

Amphibole occurs as disseminated small (< 200 μm) crystals which mostly develop at the expense of spinel (i.e. Bgt 6, Fig. 1). Its mode (1–5%) is often equal or close to the percentage of spinel. Like clinopyroxene, amphibole always occurs at triple points or

Table 1 Location, facies and textures of the xenoliths (East Carpathian, Romania)

Sample	Location	Lithology	Texture
BG 00	Bogata quarry	Clinopyroxenite	Granoblastic
BG 01	Bogata quarry	Harzburgite	Porphyroclastic
BG 02	Bogata quarry	Lherzolite	Granoblastic
BG 03	Bogata quarry	Websterite	Granoblastic
BG 04	Bogata quarry	Lherzolite	Porphyroclastic
BG 07	Bogata quarry	Lherzolite	Porphyroclastic
BG 09	Bogata quarry	Lherzolite	Porphyroclastic
BG 10	Bogata quarry	Lherzolite	Porphyroclastic
BG 15	Bogata quarry	Lherzolite	Porphyroclastic
BG 16	Bogata quarry	Lherzolite	Porphyroclastic
BG 18	Bogata quarry	Lherzolite	Granoblastic
Bgt 03	Barc quarry	Lherzolite	Granoblastic
Bgt 06	Barc quarry	Lherzolite	Porphyroclastic
Bgt 07	Barc quarry	Lherzolite	Porphyroclastic
Bgt 13	Barc quarry	Lherzolite	Porphyroclastic
Bgt 16	Barc quarry	Clinopyroxenite	Granoblastic
Bgt 17	Barc quarry	Lherzolite	Porphyroclastic
Bgt 18	Barc quarry	Lherzolite	Granoblastic
Bgt 19	Barc quarry	Lherzolite	Porphyroclastic
Bgt 21	Barc quarry	Lherzolite	Porphyroclastic
Bgt 22	Barc quarry	Lherzolite	Granoblastic
BC 01	Barc quarry	Amphibole vein	Granoblastic
BC 05	Barc quarry	Amphibole clinopyroxenite	Granoblastic
BC 09	Barc quarry	Lherzolite	Granuloblastic
Lgf 11	La Gruiu Fintina	Amphibole clinopyroxenite	Granoblastic

Bgt06   5 mm

Bgt18   5 mm

Bgt16   5 mm

BG18   5 mm

Bgt00   5 mm

⬭ Olivine with subgrain boundaries   ⬭ Orthopyroxene   ⬬ Spinel   ⬭ Clinopyroxene with twin boundaries

⬭ Amphibole   ⬬ Melt pocket

along grain boundaries but is never included in, or systematically associated with, clinopyroxene.

Evidence of melting may be found in some xenoliths, including clouded margins of clinopyroxene and amphiboles, and melt pockets filled (i.e. Bgt18, Fig. 1) with glass, euhedral crystals of spinel, olivine and clinopyroxene. In some peridotites of the BG series only, later microfractures filled by calcite, plagioclase, pyroxenes, armalcolite, apatite (Chalot-Prat et al. 1995, and Chalot-Prat F. and Arnold M. in preparation) are also observed.

If Harte's (1976) and Mercier's (1985) classifications are translated to clinopyroxenite, then clinopyroxenite (BG00), olivine clinopyroxenite (Bgt16), amphibole clinopyroxenite (Lgf11) and websterite (BG03) have a granoblastic texture. The clinopyroxenite displays nearly centimetric undeformed clinopyroxene crystals and small interstitial deformed olivine crystals (i.e. BG00, Fig. 1) which display strong lattice preferred orientation. In contrast in Bgt16 (Fig. 1), large deformed olivine crystals surrounded by large twinned clinopyroxene enclose small rounded twinned clinopyroxenes. In the amphibole clinopyroxenite (Lgf11), clinopyroxene crystals are included in large brown poikiloblastic amphiboles indicating that amphibole developed later than clinopyroxene.

The studied samples come from a relatively small (some km^2) volcanic region (Downes et al. 1995). Consequently, they could represent a sampling of the lithospheric mantle essentially along a single vertical section. The xenoliths, their textures and mineralogical characteristics have been plotted on a temperature scale (Fig. 2) using the Wood and Banno (1973) equilibrium temperature determined by Vaselli et al. (1995). Porphyroclastic textures correspond to the colder samples (BG15, BG10, BG01 and Bgt13) but as temperature increases, the grain size of recrystallized olivine

Fig. 1 Drawings after thin sections showing different textures in porphyroclastic lherzolite (Bgt6), strongly annealed porphyroclastic lherzolite (Bgt18), coarse-grained granoblastic lherzolite (BG18) and in clinopyroxenite (BG00 and Bgt16). Scales and patterns are identical for all sketches. Note the increasing grain size from Bgt6 to BG18, and the small clinopyroxenes (Bgt18 and BG18) and amphiboles (Bgt6) located at triple points and along grain boundaries

increases (BG09, BG16, BG04, BG07, Bgt06, Bgt07, Bgt17, Bgt21, Bgt03) towards granoblastic textures (BG03, Bgt18 and Bgt22). In the temperature range 1010 to 1060 °C, amphibole is present in most samples except BG09, BG07, Bgt17, BG03 and Bgt18. The samples giving the highest calculated temperature have either a granuloblastic texture (BC09, containing traces of amphibole) or a granoblastic texture (BG02 and BG18). Thus the order of increasing grain size or recrystallization, evidenced by our petrographic observations, is directly correlated to increasing equilibrium temperature.

Trace element data on whole rocks and mineral separates

Analytical techniques

Trace elements analyses were carried out using an ICP-MS (CNRS-CRPG Nancy) on whole rock powders and mineral separates prepared by Vaselli et al. (1995). In a "clean-room" laboratory, 100
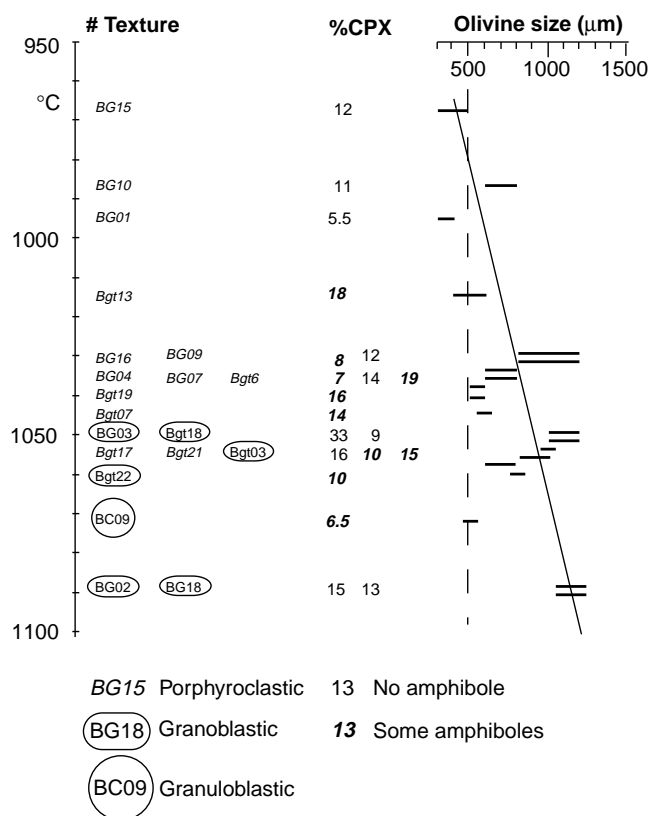
Fig. 2 Diagram showing the distribution of the samples of peridotite on a temperature scale using the temperatures calculated (Vaselli et al. 1995) from the Wood and Banno (1973) thermometer. Textures, petrographic characteristics (calculated percentage of clinopyroxene and presence of amphibole) and recrystallized olivine grain size are reported on this scale. Note the consistency of textures for samples showing similar temperatures of equilibrium, and increasing olivine grain size with increasing temperatures

Table 2 Trace element concentrations obtained by ICP-MS in international standard rocks PCC-1 (peridotite) and DTS-1 (dunite) by Ionov et al. (1992) and during this study

	PCC-1		DTS-1	
	Ionov et al. 1992	This study	Ionov et al. 1992	This study
Ba	0.68	0.87	0.3	0.40
Ce	0.057	0.044	0.05	0.049
Co		120		134
Cr		2603		3586
Cs		0.0008		0.0006
Dy	0.0013	0.0095	0.0085	0.0049
Er	0.0123	0.0112	0.0074	0.0051
Eu	0.0018	0.0011	0.0013	0.0012
Ga		0.72		0.55
Gd	0.008	0.0053	0.0063	0.0066
Hf	0.0055	0.0027	0.0046	0.0043
Ho	0.0038	0.0022	0.0016	0.0016
La	0.039	0.032	0.025	0.029
Lu	0.0049	0.0042	0.0022	0.0019
Nb	0.042	0.015	0.042	0.019
Nd	0.03	0.031	0.0272	0.027
Ni		2380		2304
Pb	8.2	7.0	7.5	8.2
Pr	0.0085	0.0076	0.0074	0.0078
Rb	0.068	0.087	0.095	0.099
Sm	0.008	0.003	0.007	0.0041
Sr	0.38	0.403	0.3	0.503
Ta	0.003	0.0148	0.0021	0.0060
Tb	0.0015	0.0013	0.001	0.0006
Th	0.0095	0.0090	0.0083	0.0085
Tm	0.0025	0.0033	0.0013	0.0013
U	0.0042	0.0068	0.0038	0.0038
V		46		15
Y		0.072		0.051
Yb	0.0215	0.020	0.01	0.008
Zr	0.13	0.115	0.11	0.012

to 200 mg of rock powder (samples and standards) or 50 to 100 mg of clean, acid-leached mineral separates were mixed with $LiBO_2$ (in proportions 1:3) in clean platinum crucibles, fused at 1080 °C and dissolved in HNO_3. Mineral separates were leached in cold HCl 2.5N for 20 min, rather than in hot HCl 6N because, as emphasized by Machado et al. (1996), Deer et al. (1993), Carignan et al. (1995) diopside is partially decomposed by heating in HCl. In any case, as already noted by Vaselli et al. (1995), clinopyroxene and amphibole separates always have a fine hyaline look. Systematic scanning electron microscope (SEM) observations of grain boundaries and intragrain sections confirm the absence of any trace of alteration around or within minerals. Quality of ICP-MS analyses was assured in analysing international peridotite standards PCC-1 and DTS-1. The results reported in Table 2 are in good agreement with those of Ionov et al. (1992). For each dissolved sample, 41 elements were analysed including 9 elements (U, Th, Ta, La, Ce, Pr, Nd, Sm, Eu) analysed in triplicate. For these elements, data are an average of these three measurements which differ by no more than 5%. Most of the REE data are similar (1–10% difference) to those obtained by isotopic dilution on clinopyroxenes and amphiboles by Vaselli et al. (1995), even for samples with the lowest contents. Some LREE data (in 4 clinopyroxenes out of 23) differ by 15 to 25% relative to the data of Vaselli et al. (1995) while the ratios between REE remain the same. As whole rocks, clinopyroxenes and amphiboles from the same series were analysed at the same time, these differences cannot be ascribed to changes in our analytical conditions and suggest instead slight heterogeneities in the clinopyroxene aliquots. In addition Gd appears to have often been

slightly underestimated by ICP-MS accounting for the slight negative Gd anomaly on a number of mantle-normalized spidergrams. These small inconsistencies do not have any significant effects on the form of the mantle-normalized patterns, nor on the mass balance calculations between whole rocks and clinopyroxenes. Note that the Rb contents of cpx obtained by ICP-MS are much higher than those obtained by Vaselli et al. (1995) by isotopic dilution after leaching in hot HCl, while the Sr contents are comparable to their results. This Rb loss may be attributed to a too aggressive leaching which induced a selective separation of the largest atoms from cpx crystals. Lead data, only reported for 14 whole-rock powders on 22 studied samples, will not be used in this study. Indeed a slight Pb pollution of platine crucibles acquired during their stockage has been recognized well after the former analyses were performed and led us to get new analyses on the samples where enough powder remained. Note also that if K and Ti concentrations in whole rocks (data in Vaselli et al. 1995) are, though low, above the detection limits by X-ray fluorescence (XRF) for Ti, and by atomic absorption spectrometry (AAS) for K, it is not the case in clinopyroxene, particularly for K often below the detection limit by Electron MicroProbe Analysis (EMPA). Nevertheless the validity of the data is confirmed by two facts: (1) our own measures of Ti and K by EMPA (SX 50, University of Nancy; beam current: 5.9 A; accelerating voltage: 15.0 V; counting time: 10 s) on clinopyroxenes and interstitial amphiboles agree with those of Vaselli; (2) comparisons between EMPA and ion probe (SIMS) data on amphiboles (in Vaselli et al. 1995) show that whatever the analytical method, a significant difference of K_2O and Ti_2O contents persists between amphiboles of veins and interstitial amphiboles of peridotites. So the K and Ti contents reported in the PM-normalized spidergrams of clinopyroxenes, interstitial amphiboles and

bulk rocks are assumed to be correct. Trace element analyses of a few low-SiO$_2$ calc-alkaline lavas (Mason et al. 1996) were carried out by routine analysis on the ICP-MS of CNRS-CRPG.

Trace element data

Results are listed in Table 3a–d for whole rocks, clinopyroxene and amphibole separates from 24 xenoliths (BG, Bgt, BC and Lgf series, in Table 1). In the mantle-normalized incompatible element diagrams, the sequence of elements corresponds to the order of decreasing incompatibility during melting processes of a "normal" mantle (Hofmann 1988). The trace element contents of Primitive Mantle (PM) are also taken from Hofmann (1988). The K and Ti contents for whole rocks and mineral separates are taken from Vaselli et al. (1995).

The whole-rock samples (Fig. 3) of peridotites and veins are fundamentally distinct. The peridotites (group I: lherzolites, websterite and harzburgite) are all depleted in most incompatible trace elements relative to PM (except U and Rb), while the veins (group II: amphibole clinopyroxenites, amphibole veins and clinopyroxenites) are enriched in all incompatible trace elements.

However group I does not display the LILE (large ion lithophile element) -depleted patterns which would result from simple melt extraction as suggested by the LREE-depleted spidergrams of clinopyroxenes. Indeed both clinopyroxene separates and whole rocks (Fig. 4) are strongly enriched not only in Rb and U but also in Th, Ba and sometimes in LREE. The only exceptions to this enrichment are K and, in porphyroclastic and most of the granoblastic samples, Ta and Nb.

In detail, based on the trace element patterns, three subgroups can be discerned within the *group I*, namely using the terminology of Fig. 2: (1) the porphyroclastic lherzolites (BG 04/07/10/15/16; Bgt 6/7/13/17/19/21), the granoblastic lherzolites with an intermediate equilibrium temperature (IT granoblastic: Bgt 03/18/22) and the websterite (BG 03) (Figs. 3a,b; 4a,b); (2) the porphyroclastic harzburgite (BG 01) (Figs. 3a and 4a); (3) the granoblastic lherzolites with the highest equilibrium temperature (HT granoblastic: BG 02/18) (Figs. 3c and 4c); and two sub-groups in *group II* with: (1) the amphibole pyroxenites (Lgf11, BC05) and veins (BC01); (2) the clinopyroxenites (BG00, Bgt16) (Figs. 3d and 4d).

Group I

1. *Porphyroclastic and intermediate temperature (IT) granoblastic lherzolites, and websterite (Figs. 3a,b; 4a,b).* These whole-rocks display great regularity in their spidergrams, with negative anomalies in Ta and Nb, a strong positive anomaly in U and also a relative enrichment in Rb, Ba, and Th [(Th/Ta)$_N$ > 1; N = normalized value]. Their (LREE/HREE)$_N$ ratios

are mostly lower than 1, but sometimes equal to or slightly higher than 1. On the whole the most LREE-poor rocks are also the most Ta- and Nb-poor. The clinopyroxene patterns are also very similar from one sample to another. They closely reflect, in terms of trace element ratios, those of their whole-rocks so that clinopyroxene can be considered as the main trace element-bearing phase in these peridotites. This is more obvious in the Bgt series, where the xenoliths also display a good textural homogeneity. Nevertheless in detail, the clinopyroxene spidergrams differ slightly from those of their whole-rocks in having lower Ba and often Nb contents, partly due to the very low partition coefficients of clinopyroxene for these elements (Table 4), and also a slight negative anomaly in Ti and an absence of a Sr anomaly. Note that the interstitial amphiboles (data in Vaselli et al. 1995) have, as do the coexisting clinopyroxenes, relatively low K, Nb, Ti and Zr contents and a similar LREE-depleted pattern. Mass balance calculations between whole-rocks and clinopyroxene suggest that, in some samples of the BG series, some other phases, observed in later fissures, are the main specific hosts not only of Rb, Th and U but also of LREE, Ta, Ti and Sr (Chalot-Prat et al. 1995, and Chalot-Prat F and Arnold M in preparation).

The websterite (BG 03) and its clinopyroxenes differ from the porphyroclastic and IT granoblastic lherzolites only by having a higher trace element content, slightly higher than that of the PM.

2. *Porphyroclastic harzburgite (Figs. 3a and 4a).* The total whole-rock trace element content of harzburgite is much lower than that of the lherzolites. Nevertheless its pattern is similar to those of the porphyroclastic facies with positive anomalies in Rb, Th, U and Sr, and a negative anomaly in Ta but not in Nb. Furthermore, contents of most of these elements (to the left of La in the pattern) are the same as in some of the porphyroclastic rocks. The same remarks apply to the harzburgite clinopyroxenes. Both whole-rock and clinopyroxenes display a strong negative anomaly in Ti. In contrast, while the whole-rock displays a slight U-shaped REE pattern, the clinopyroxenes display a LREE-depleted pattern. Mass balance calculations demonstrate once more that other Rb, Th, U, Ta and LREE-bearing phases occur in this rock, which is confirmed by observations of the filling of fissures of this harzburgite (Chalot-Prat et al., op.cit.).

3. *High temperature (HT) granoblastic lherzolites (Figs. 3c and 4c).* The HT granoblastic whole-rocks display a more regular pattern than porphyroclastic and IT granoblastic rocks with, apart from a high U content, a gradual enrichment in the most incompatible trace elements without any Ta anomaly [(Th/Ta)$_N$ around 1]. The clinopyroxene patterns also show a positive U anomaly but contrast with those of their whole-rocks since they are LREE-poor and display a negative Ti anomaly. These slight differences could

Table 3 a Trace element (ppm) analyses of whole-rocks (wr) of BG series xenoliths (Eastern Transylvanian Basin, Romania)

	BG-00 (wr)	BG-01(wr)	BG-02 (wr)	BG-03 (wr)	BG-04 (wr)	BG-07 (wr)	BG 09 (wr)	BG-10 (wr)	BG-15 (wr)	BG-16 (wr)	BG-18 (wr)
Ba	12.22	0.74	11.51	5.76	2.37	7.06	3.85	0.42	2.45	13.95	9.728
Ce	6.994	0.162	1.797	2.117	0.440	0.794	0.853	0.299	0.356	0.330	1.322
Co	181	104	95	62	99	93	93	97	95	98	96
Cr	1127	2432	3293	3987	2361	2697	2920	3116	2737	2386	2787
Cs	0.0678	0.0573	0.0756	0.0704	0.0813	0.1025	0.1289	0.1254	0.1506	0.1458	0.1817
Dy	2.285	0.045	0.419	1.100	0.245	0.470	0.416	0.321	0.467	0.284	0.336
Er	1.222	0.033	0.292	0.765	0.161	0.333	0.245	0.218	0.279	0.170	0.208
Eu	0.829	0.011	0.109	0.277	0.058	0.108	0.090	0.071	0.092	0.070	0.087
Ga	8.55	0.98	3.11	7.04	1.81	3.48	3.21	2.56	2.67	1.92	2.99
Gd	2.165	0.027	0.303	0.846	0.154	0.355	0.286	0.218	0.284	0.231	0.294
Hf	0.923	0.029	0.143	0.397	0.125	0.163	0.163	0.115	0.149	0.101	0.170
Ho	0.479	0.010	0.088	0.273	0.063	0.120	0.105	0.080	0.101	0.063	0.076
La	2.186	0.139	0.867	0.717	0.173	0.327	0.509	0.108	0.108	0.514	0.614
Lu	0.1451	0.0071	0.0515	0.1215	0.0313	0.0595	0.0420	0.0402	0.0515	0.0350	0.0353
Nb	0.787	0.190	0.921	0.418	0.099	0.139	0.400	0.166	0.084	0.177	0.702
Nd	6.99	0.12	1.00	2.05	0.39	0.73	0.72	0.44	0.47	0.72	0.81
Ni	506	2576	2023	1179	2284	1988	2058	2160	2248	2282	2093
Pb	0.3029	/	0.2245	0.2743	0.4107	0.1990	0.3146	/	0.1025	0.1488	0.1568
Pr	1.218	0.022	0.229	0.354	0.072	0.124	0.129	0.060	0.071	0.148	0.174
Rb	0.539	0.312	1.123	1.004	0.383	1.074	0.728	0.741	0.594	0.557	1.508
Sm	2.170	0.031	0.288	0.671	0.148	0.267	0.207	0.165	0.201	0.195	0.229
Sr	65.3	6.6	20.6	33.7	6.2	10.6	12.5	7.2	8.4	4.2	18.6
Ta	0.0919	0.0042	0.0654	0.0244	0.0040	0.0094	0.0170	0.0036	0.0024	0.0042	0.0467
Tb	0.351	0.004	0.055	0.164	0.036	0.068	0.062	0.040	0.054	0.043	0.049
Th	0.1156	0.0215	0.1221	0.0655	0.0289	0.0448	0.0531	0.0110	0.0102	0.0136	0.0696
Tm	0.1651	0.0074	0.0381	0.1069	0.0259	0.0466	0.0481	0.0354	0.0392	0.0259	0.0296
U	0.0506	0.0289	0.0994	0.0502	0.0221	0.0251	0.0511	0.0323	0.0173	0.0180	0.0584
V	273	30	64	139	46	70	64	59	61	48	58
Y	12.55	0.23	2.61	6.94	1.54	3.02	2.71	2.11	2.83	1.76	2.02
Yb	1.02	0.03	0.27	0.71	0.14	0.31	0.27	0.21	0.30	0.19	0.20
Zr	26.1	1.5	7.0	13.7	4.1	6.7	6.1	4.1	5.2	3.2	5.8

Table 3 b Trace element (ppm) analyses of clinopyroxenes (cpx) from BG series xenoliths (Eastern Transylvanian Basin, Romania)
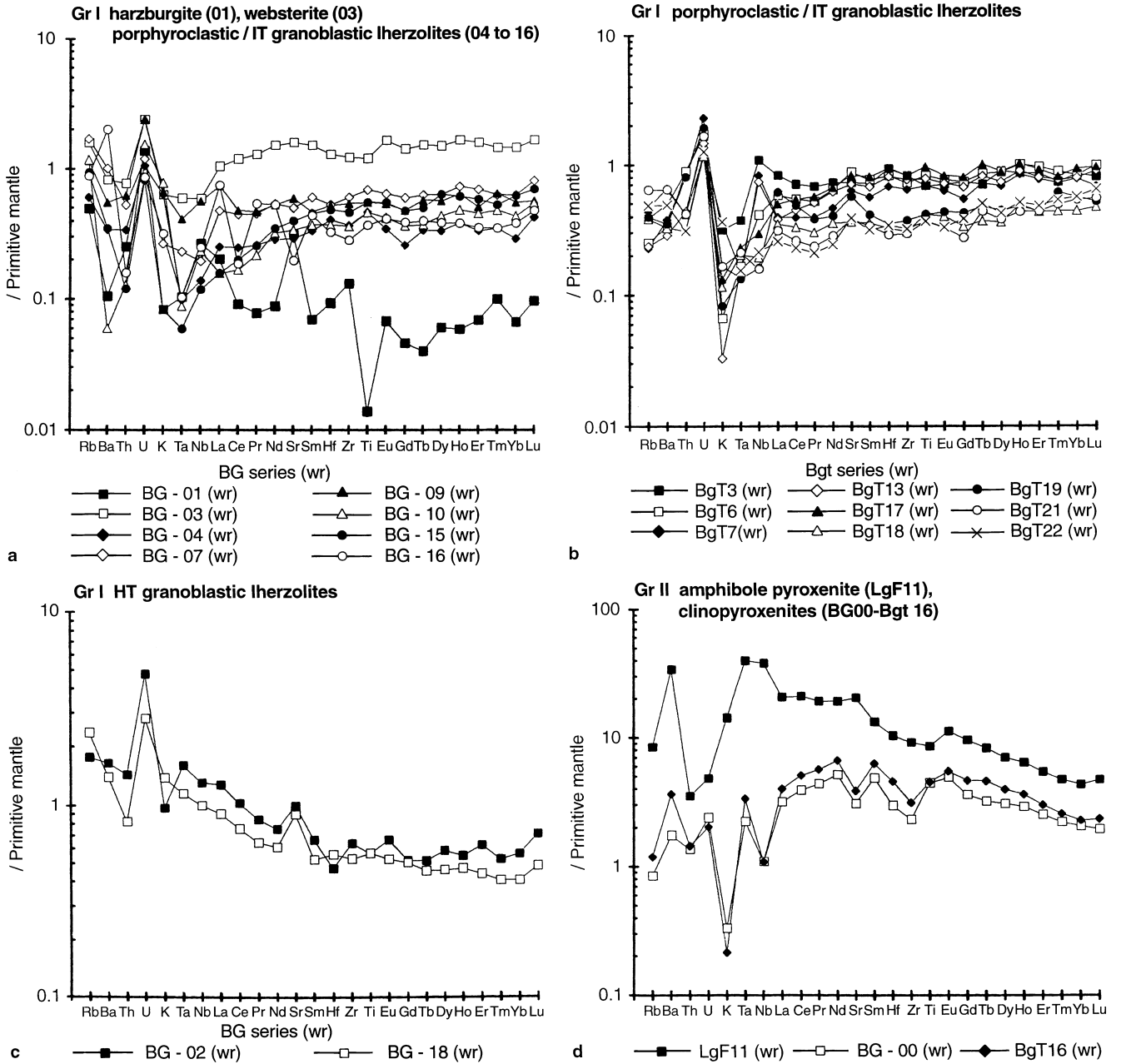
	BG-00(cpx)	BG-01(cpx)	BG-02(cpx)	BG-03(cpx)	BG-04(cpx)	BG-07(cpx)	BG-09(cpx)	BG-10(cpx)	BG-15(cpx)	BG-16(cpx)	BG-18(cpx)
Ba	1.93	0.95	2.39	1.15	0.53	0.78	0.79	0.74	0.87	1.33	2.79
Ce	6.84	1.39	4.16	4.07	4.81	3.71	5.47	2.51	2.15	2.51	5.22
Co	27	29	20	19	18	19	20	18	18	17	19
Cr	1112	6200	6008	3171	5997	4375	5706	5368	4242	5026	5475
Cs	0.204	0.141	0.137	0.118	0.189	0.133	0.138	0.215	0.218	0.173	0.251
Dy	2.63	0.57	2.60	3.00	2.72	3.37	3.18	2.83	2.82	2.59	2.65
Er	1.30	0.40	1.52	1.90	1.64	2.06	1.93	1.68	1.73	1.60	1.55
Eu	0.770	0.175	0.541	0.685	0.640	0.683	0.746	0.614	0.581	0.542	0.646
Ga	9.25	1.97	4.12	4.21	3.80	4.40	5.14	3.48	3.46	3.34	4.48
Gd	2.25	0.44	1.86	2.08	1.94	2.12	2.18	1.94	1.87	1.60	1.95
Hf	1.05	0.25	0.79	1.14	1.03	1.11	1.02	0.85	0.92	0.80	0.78
Ho	0.551	0.137	0.587	0.724	0.601	0.725	0.767	0.644	0.673	0.607	0.602
La	1.98	0.58	1.35	1.09	1.68	1.29	2.22	0.58	0.53	0.69	1.71
Lu	0.164	0.068	0.203	0.267	0.218	0.274	0.257	0.256	0.240	0.224	0.219
Nb	0.575	0.177	0.543	0.075	0.068	0.087	0.094	0.098	0.034	0.089	0.488
Nd	6.87	1.51	3.76	4.51	4.42	4.20	4.98	3.17	3.19	2.97	4.81
Ni	238	588	369	364	333	327	349	351	341	305	340
Pr	1.234	0.217	0.703	0.772	0.820	0.656	0.818	0.526	0.453	0.479	0.899
Rb	0.726	0.599	0.509	0.438	0.669	0.494	1.097	0.783	0.815	0.566	0.929
Sm	2.30	0.53	1.42	1.81	1.64	1.73	1.81	1.45	1.44	1.45	1.62
Sr	72	31	83	80	69	63	86	55	43	47	92
Ta	0.0837	0.0183	0.0680	0.0129	0.0130	0.0216	0.0631	0.0139	0.0057	0.0135	0.0642
Tb	0.420	0.090	0.378	0.429	0.398	0.465	0.469	0.412	0.413	0.372	0.413
Th	0.0810	0.0646	0.1144	0.0626	0.2531	0.0394	0.3344	0.1236	0.0847	0.0888	0.1106
Tm	0.180	0.069	0.209	0.286	0.228	0.284	0.292	0.268	0.249	0.226	0.227
U	0.0530	0.0848	0.0857	0.0462	0.1061	0.0284	0.2855	0.0941	0.0688	0.0674	0.0641
V	269	179	208	198	213	212	246	212	170	201	194
Y	13.54	3.60	15.84	18.78	15.66	19.44	20.56	17.55	17.12	15.46	15.83
Yb	1.09	0.44	1.43	1.86	1.47	1.96	1.93	1.66	1.73	1.56	1.45
Zr	28	11	25	34	36	36	34	29	29	25	27

Table 3 c Trace element (ppm) analyses of whole-rocks (wr) of Bgt and Lgf series xenoliths (Eastern Transylvanian Basin, Romania)

	BgT3 (wr)	BgT6 (wr)	BgT7 (wr)	BgT13 (wr)	BgT16 (wr)	BgT17 (wr)	BgT18 (wr)	BgT19 (wr)	BgT21 (wr)	BgT22 (wr)	LgF11 (wr)
Ba	3.47	2.34	2.63	2.00	25.68	4.63	2.29	2.46	4.52	3.44	236.98
Ce	1.25	0.96	0.70	0.80	9.10	0.96	0.58	0.87	0.46	0.41	37.63
Co	71	73	75	75	50	71	80	80	82	85	37
Cr	2337	2810	2193	2219	560	2043	2150	2135	2030	1722	430
Cs	0.024	0.022	0.028	0.032	0.049	0.034	0.057	0.051	0.065	0.054	0.122
Dy	0.661	0.651	0.507	0.545	2.963	0.654	0.267	0.330	0.280	0.315	5.218
Er	0.412	0.462	0.370	0.385	1.462	0.443	0.209	0.211	0.212	0.232	2.638
Eu	0.119	0.128	0.107	0.121	0.934	0.139	0.067	0.073	0.055	0.056	1.911
Ga	3.13	3.93	3.28	3.51	9.70	4.21	2.59	2.48	2.00	2.14	16.43
Gd	0.441	0.439	0.327	0.404	2.799	0.479	0.200	0.255	0.164	0.229	5.767
Hf	0.290	0.256	0.210	0.252	1.425	0.293	0.101	0.109	0.090	0.106	3.225
Ho	0.141	0.165	0.138	0.148	0.601	0.168	0.081	0.079	0.071	0.084	1.059
La	0.571	0.401	0.271	0.262	2.770	0.344	0.239	0.423	0.213	0.178	14.261
Lu	0.0597	0.0729	0.0503	0.0663	0.1753	0.0712	0.0347	0.0385	0.041	0.0479	0.3538
Nb	0.777	0.295	0.591	0.529	0.779	0.212	0.139	0.115	0.114	0.153	27.079
Nd	0.993	0.875	0.633	0.846	9.076	0.905	0.483	0.549	0.385	0.333	26.147
Ni	1493	1503	1572	1545	444	1371	1696	1744	1804	1865	194
Pb	0.3251			0.1185	0.0729					0.3650	0.9724
Pr	0.188	0.144	0.110	0.142	1.576	0.158	0.084	0.107	0.065	0.058	5.344
Rb	0.246	0.160	0.146	0.150	0.760	0.293	0.244	0.253	0.405	0.310	5.354
Sm	0.319	0.344	0.251	0.302	2.814	0.361	0.159	0.186	0.151	0.140	5.980
Sr	15.5	18.6	13.4	15.1	82.0	17.6	7.7	12.1	8.0	8.2	434.3
Ta	0.0154	0.0069	0.0056	0.0063	0.1388	0.0096	0.0084	0.0055	0.0087	0.0063	1.6326
Tb	0.0763	0.0926	0.0781	0.0885	0.5032	0.1100	0.0400	0.0520	0.0473	0.0548	0.9059
Th	0.0746	0.0758	0.0678	0.0372	0.1237	0.0353	0.0263	0.0687	0.0358	0.0265	0.3017
Tm	0.0545	0.0656	0.0539	0.0568	0.1919	0.0601	0.0325	0.0455	0.0367	0.0396	0.3536
U	0.0345	0.0366	0.0483	0.0308	0.0429	0.0250	0.0249	0.0404	0.0351	0.0266	0.1023
V	59	71	58	63	225	74	42	45	45	42	199
Y	3.44	3.84	3.24	3.45	14.37	4.03	1.82	2.08	1.78	2.08	25.21
Yb	0.417	0.408	0.384	0.390	1.133	0.464	0.218	0.277	0.265	0.281	2.154
Zr	9.3	8.1	7.2	8.7	35.1	9.3	3.4	4.2	3.3	3.6	103.9

Table 3 d Trace element (ppm) analyses of clinopyroxenes (cpx) and amphiboles (amph) from xenoliths of the Bgt, Lgf and BC series (Eastern Transylvanian Basin, Romania)

	BgT3(cpx)	BgT6(cpx)	BgT7(cpx)	BgT13(cpx)	BgT16(cpx)	BgT17(cpx)	Bgt18(cpx)	BgT19(cpx)	BgT21(cpx)	BgT22(cpx)	Lgf11(amph)	BC05(amp-h)	BC05(cpx)	BC01(amp-h)
Ba	0.541	0.449	0.55	0.537	1.507	1.995	0.675	0.96	0.835	1.569	308	238	20.762	301
Ce	4.63	3.62	5.58	6.4	10.34	5.25	6.21	10.46	5.49	4.21	37.4	23.05	16.98	18.15
Co	20	21	21	21	31	24	468	21	23	24	54	54	31	50
Cr	5036	5426	5227	5158	765	4870	6453	6651	6871	5978	585	672	591	741
Cs	0.039	0.044	0.062	0.06	0.074	0.099	0.07	0.106	0.123	0.144	0.126	0.089	0.34	0.112
Dy	3.04	2.7	2.93	3.14	3.43	3.74	2.78	2.7	2.59	2.57	4.83	3.93	3.02	3.79
Er	1.9	1.65	1.85	1.9	1.69	2.23	1.72	1.77	1.69	1.73	2.44	2.03	1.62	1.81
Eu	0.723	0.624	0.67	0.739	1.155	0.853	0.599	0.656	0.555	0.542	2.039	1.629	1.165	1.516
Ga	4.08	4.7	4.95	4.92	12.18	5.72	4.81	4.5	4.39	4.61	19.83	19.75	12.88	16.56
Gd	2.28	2.04	2.17	2.36	3.48	2.61	1.95	2	1.78	1.76	5.53	4.01	3.1	4.03
Hf	1.13	0.89	1.02	1.22	1.65	1.35	0.72	0.75	0.58	0.71	2.46	1.77	2.15	2.57
Ho	0.775	0.701	0.72	0.76	0.76	0.862	0.713	0.701	0.683	0.695	1.044	0.821	0.723	0.81
La	1.52	1.52	2.66	2.64	3.1	1.77	2.61	5.2	2.41	1.77	13.95	8.4	5.79	5.84
Lu	0.288	0.272	0.275	0.296	0.204	0.321	0.255	0.265	0.252	0.261	0.309	0.277	0.268	0.234
Nb	0.133	0.077	0.131	0.127	0.798	0.15	0.242	0.128	0.165	0.177	37.688	21.997	1.501	16.153
Nd	4.95	3.77	4.23	5.17	10.34	5.4	4.28	5.58	4.07	3.34	25.43	17.73	13.21	16.15
Ni	359	361	368	366	210	406	668	373	408	429	304	241	122	326
Pr	0.819	0.612	0.812	0.964	1.789	0.914	0.814	1.217	0.755	0.597	5.319	3.476	2.618	2.936
Rb	0.257	0.752	0.386	0.293	0.387	0.524	0.308	0.506	0.605	0.884	4.404	7.152	1.86	6.41
Sm	1.9	1.6	1.63	1.91	3.36	2.22	1.55	1.78	1.47	1.4	6.27	4.72	3.67	4.63
Sr	50	49	59	78	96	84	73	107	83	67	469	502	179	570
Ta	0.0207	0.0177	0.0131	0.0135	0.156	0.0212	0.0198	0.0193	0.0199	0.0249	2.2215	1.2266	0.1303	0.9556
Tb	0.443	0.379	0.422	0.439	0.582	0.535	0.385	0.398	0.35	0.361	0.838	0.632	0.514	0.659
Th	0.302	0.437	1.305	0.335	0.109	0.191	0.227	0.675	0.317	0.233	0.237	0.288	0.276	0.24
Tm	0.301	0.246	0.288	0.295	0.237	0.312	0.257	0.277	0.254	0.264	0.355	0.29	0.25	0.246
U	0.134	0.166	0.413	0.152	0.058	0.104	0.072	0.199	0.109	0.122	0.089	0.09	0.177	0.288
V	240	245	246	261	352	265	251	260	267	247	302	296	198	428
Y	18.9	16.7	18.7	19.8	18.6	22.2	17.3	17.9	17	17.7	25.9	21.5	17.4	20.6
Yb	1.82	1.57	1.81	1.83	1.44	2.01	1.58	1.68	1.64	1.72	2.03	1.83	1.49	1.53
Zr	41	33	38	47	47	46	24	33	23	27	98	68	65	94

Gr I harzburgite (01), websterite (03) porphyroclastic / IT granoblastic lherzolites (04 to 16)

Gr I porphyroclastic / IT granoblastic lherzolites

Gr I HT granoblastic lherzolites

Gr II amphibole pyroxenite (LgF11), clinopyroxenites (BG00-Bgt 16)
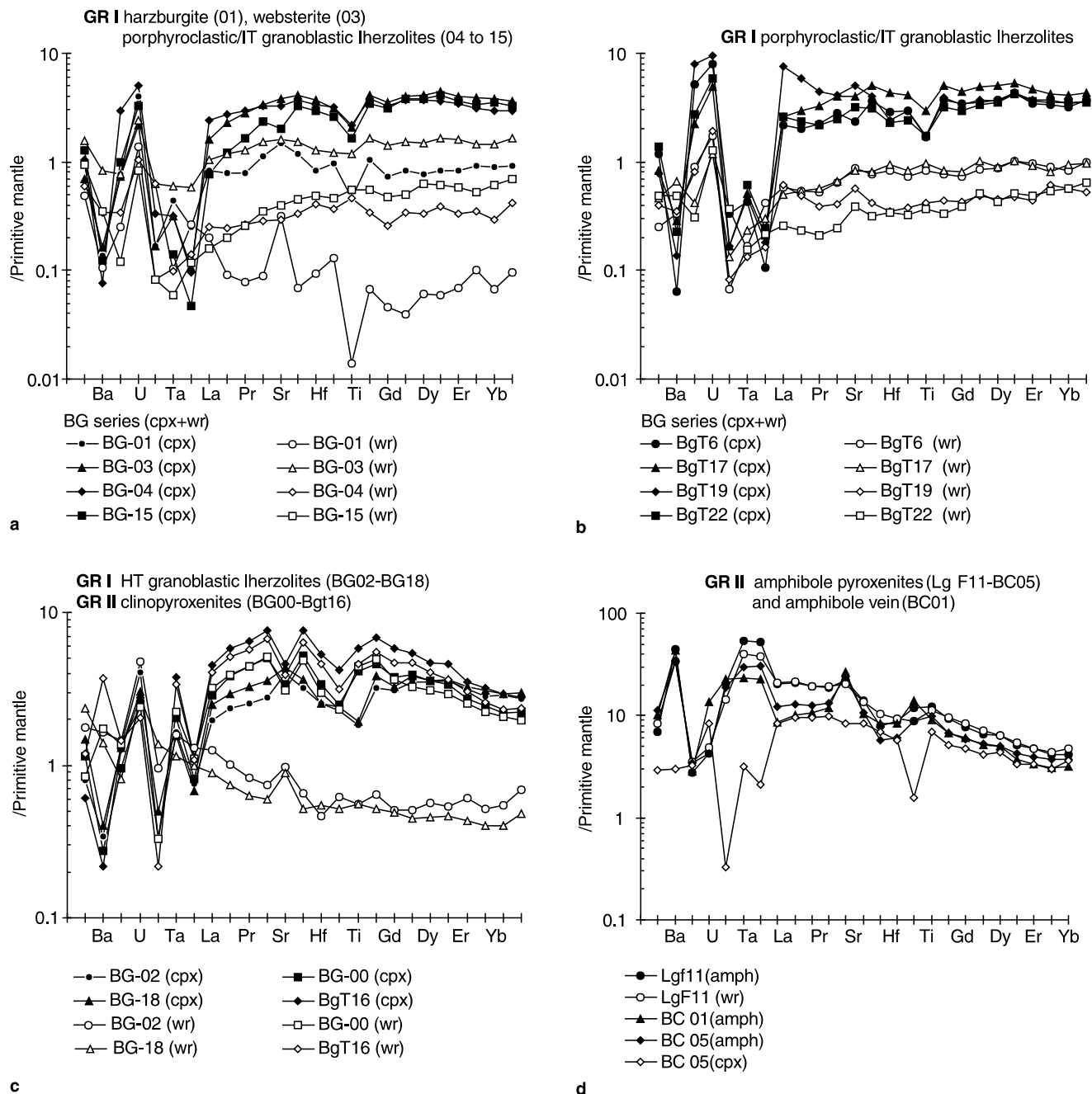
Fig. 3a–d PM-normalized spidergrams of whole-rocks from: **a** harzburgite (BG-01), websterite (BG-03), porphyroclastic and I*T* (intermediate temperature) granoblastic lherzolites of the BG series; **b** porphyroclastic and I*T* granoblastic lherzolites of the Bgt series; **c** H*T* (high temperature) granoblastic lherzolites; **d** clinopyroxenites (BG-00, Bgt16) and amphibole pyroxenite (Lgf11)

be explained by the abundance of LREE-, Ta- and Ti- bearing phases in the later fissures. In addition the clinopyroxene have relatively high Ta contents compared to clinopyroxene of porphyroclastic rocks. In fact, the clinopyroxene spidergrams are intermediate between those of porphyroclastic rocks and those of clino-pyroxenites (see below). The same remark can be made with respect to the major elements since these clinopy-roxenes are as Ti-poor, and Cr- and Na- rich as those of porphyroclastic rocks, but slightly more enriched in Al

and Fe, elements which allow discrimination from the clinopyroxenes of clinopyroxenites.

Group II

1. Amphibole clinopyroxenites and amphibole veins (Figs. 3d and 4d). Amphibole from amphibole vein (BC 01) and clinopyroxenites (BC 05 and Lgf 11) have very similar PM-normalized patterns: strongly depleted in Th and U, slightly depleted in Zr and Hf, and enriched in all other incompatible trace elements, particularly Ba, K, Ta and Nb, which is partly due to the partition coefficients of amphibole for these elements (Table 4). In the amphibole clinopyroxenite (Lgf 11), the trace element composition of the whole-rock is controlled by amphibole as indicated by

GR I harzburgite (01), websterite (03)
porphyroclastic/IT granoblastic lherzolites (04 to 15)

GR I porphyroclastic/IT granoblastic lherzolites

BG series (cpx+wr)
- —●— BG-01 (cpx)
- —○— BG-01 (wr)
- —▲— BG-03 (cpx)
- —△— BG-03 (wr)
- —◆— BG-04 (cpx)
- —◇— BG-04 (wr)
- —■— BG-15 (cpx)
- —□— BG-15 (wr)

a

BG series (cpx+wr)
- —●— BgT6 (cpx)
- —○— BgT6 (wr)
- —▲— BgT17 (cpx)
- —△— BgT17 (wr)
- —◆— BgT19 (cpx)
- —◇— BgT19 (wr)
- —■— BgT22 (cpx)
- —□— BgT22 (wr)

b

GR I HT granoblastic lherzolites (BG02-BG18)
GR II clinopyroxenites (BG00-Bgt16)

GR II amphibole pyroxenites (Lg F11-BC05)
and amphibole vein (BC01)

- —●— BG-02 (cpx)
- —■— BG-00 (cpx)
- —▲— BG-18 (cpx)
- —◆— BgT16 (cpx)
- —○— BG-02 (wr)
- —□— BG-00 (wr)
- —△— BG-18 (wr)
- —◇— BgT16 (wr)

c

- —●— Lgf11(amph)
- —○— LgF11 (wr)
- —▲— BC 01(amph)
- —◆— BC 05(amph)
- —◇— BC 05(cpx)

d

Fig. 4a–d PM-normalized spidergrams of clinopyroxenes and/or amphiboles and their host whole rocks for comparison: **a** harzburgite (BG-01), websterite (BG-03), porphyroclastic and I*T* granoblastic lherzolites of the BG series; **b** porphyroclastic lherzolites and I*T* granoblastic lherzolites of the Bgt series; **c** H*T* granoblastic lherzolites (BG-02, BG-18) and clinopyroxenites (BG-00, Bgt16); **d** amphibole pyroxenites (Lgf11, BC 05) and vein (BC 01)

the superposition of their spectra. The trace element spidergrams of amphiboles and clinopyroxenes from amphibole clinopyroxenite (BC 05) are quite different, despite the fact that their REE patterns superpose. Compared with the amphiboles, the clinopyroxenes are richer in U and strongly depleted in K, Ta [(Th/Ta)$_N$ > 1], Nb and Ti with a relatively high (La/Ta)$_N$

ratio. They are rather comparable to clinopyroxenes of the porphyroclastic facies as it would be expected from major element compositions (Vaselli et al. 1995). The only difference is an enrichment in Fe (from about 3 to 6.5% FeO) counterbalanced by a depletion in Mg (from 15 to 13% MgO) and in Cr (from 1 to 0.1% Cr$_2$O$_3$), features more common in clinopyroxene from clinopyroxenites. Amphibole which occurs in veins and amphibole pyroxenites (data in Vaselli et al. 1995) strongly differs from interstitial amphibole of the porphyroclastic facies, with higher Nb, LREE, Al, Fe, Ti and K (but not Na) contents. Note that olivine of the amphibole clinopyroxenite (Lgf 11) has a lower Mg/Fe ratio than in lherzolites.

Table 4 Partition coefficients used for calculating the trace element compositions of liquids in equilibrium with metasomatic clinopyroxenes and amphiboles (see text for information about references)

	$D^{cpx/melt}$	$D^{amph/melt}$
Rb	0.004	0.220
Ba	0.0009	0.278
Th	0.006	0.007
K	0.0072	1.36
Ta	0.010	0.074
Nb	0.005	0.050
La	0.065	0.075
Ce	0.097	0.108
Pb	0.072	0.040
Sr	0.079	0.376
Nd	0.203	0.221
Zr	0.122	0.124
Hf	0.256	0.331
Sm	0.289	0.323
Eu	0.327	0.366
Ti	0.384	0.717
Gd	0.339	0.537
Tb	0.364	0.427
Dy	0.376	0.459
Er	0.352	0.393
Yb	0.372	0.250
Lu	0.350	0.380

2. Clinopyroxenites (Figs 3d & 4c). The spidergrams of whole rocks and clinopyroxenes (BG 00, Bgt 16) resemble each other apart from Rb and Ba, which is due to very low partition coefficients of clinopyroxene for these elements. These patterns are slightly convex upward with negative anomalies in K, Nb, Sr, Zr and Hf. As already noted, the trace element spidergrams of clinopyroxenes from anhydrous clinopyroxenites are different from those of clinopyroxenes from amphibole clinopyroxenites, porphyroclastic lherzolites or the websterite. In terms of major elements, they are systematically richer in Ti, Al and Fe, but poorer in Mg and Cr compared to those of porphyroclastic lherzolites. This enrichment in Fe compensating for a depletion in Mg is also found in olivines, as in amphibole pyroxenites (Vaselli et al. 1995). These differences are the same as those existing between amphiboles from veins and peridotites, which suggests a genetic link between clinopyroxenites and amphibole veins.

Petrographical and geochemical evidence for two different metasomatic events

Petrographical evidence

Using the textures of the xenoliths and their positions on a temperature scale, it is possible to decipher a number of points:

1. When formed by subgrain rotation, the size of dynamically recrystallized olivine crystals may be correlated to the applied stress (Mercier 1985) and is homogeneous in a single sample. However, as the distribution of grain size is variable in some xenoliths studied (Fig. 2), grain boundary migration probably took place in these rocks. This process is temperature enhanced (Urai et al. 1986) and is also supported by the straight or slightly curved olivine-olivine grain boundaries and the observation that the size of recrystallized olivine increases with increasing temperature (Fig. 2).

2. Amphibole and clinopyroxene are scattered throughout the lherzolites, isolated from each other and developed along grain boundaries, which precludes any subsolidus re-equilibration process between them. They have similar habits to clinopyroxene described from infiltrated dunites in ophiolites (Nicolas and Prinzhofer 1983; Hoxha 1993). Therefore, as in dunites and, by comparison with experiments performed by Watson (1982) and Riley and Kohlstedt (1991), we consider that the interstitial amphiboles and clinopyroxenes in Persani Mts peridotite xenoliths are metasomatic and formed within an original harzburgite or a diopside-poor lherzolite. The infiltration of a melt may have enhanced the process of grain boundary migration of the dynamically recrystallized olivine (Urai et al. 1986). Grain boundary migration as well as fast diffusion (Jurewicz and Watson 1988) may explain the absence of any compositional gradient (Vaselli et al. 1995) within these minerals and, therefore, of any imprint of the melt infiltration on the grain margins. This implies that the infiltration process took place in the mantle before the xenoliths were brought up to the surface.

3. With higher volume of melt reacting with peridotites, clinopyroxenites, amphibole clinopyroxenites and amphibole veins, were formed. Their textures are very similar to those described by Nicolas and Prinzhoffer (1983) from the transition zone of ophiolites. In the clinopyroxenites, diopside developed at the expense of olivine and rare enstatite, while the presence of twinned clinopyroxenes implies that some crystals are magmatic. Indeed some are included within deformed olivine and are interpreted as resulting from the impregnation of a disrupted sponge-like coarse-grained peridotite in the process of resorption. Amphiboles in amphibole clinopyroxenites developed later than, and at the expense of, clinopyroxenes around which they crystallized.

3. Thus two types of melt infiltration may have occurred either by impregnation along grain boundaries yielding the small clinopyroxenes and amphiboles or by percolation through fracture systems in which the melt was channelled and crystallized yielding clinopyroxenites or amphibole-bearing clinopyroxenites and amphibole veins.

Geochemical evidence

The trace element compositions of whole rocks and separate clinopyroxenes of peridotites and veins entirely

support and even constrain the hypothesis of successive melt infiltrations. Our demonstration is based on a concept of physico-chemical processes involved in mantle metasomatism, which needs to be presented briefly. From our point of view, metasomatic minerals in the peridotites (group I) result from transformation of pre-existing minerals which have reacted with a percolating melt because they were not in equilibrium with it. The formation of metasomatic minerals has thus restored equilibrium between the host rock and the melt. There is thus no need of further re-equilibration with trace element diffusion between the metasomatic minerals and the host minerals as assumed by Bodinier et al. (1990), Rampone et al. (1993), Vaselli et al. (1995), Vanucci et al. (1995), Lee et al. (1996) and Zanetti et al. (in press). The absence of trace element transfer is also supported by mass balance calculations between whole rocks and diopside (and amphibole) which attest for a negligible content in trace elements of other minerals of peridotites. There is also no more major element transfer as attested by an absence of any compositional zonation within neighbouring metasomatic and host minerals or any significant compositional change in the host minerals (data in Vaselli et al. 1995), even when the compositional gradients in major elements are much higher than in trace elements.

These above considerations rule out the origin of trace element signature of amphibole and diopside by subsolidus reaction with olivine, enstatite and spinel. Because diopside and amphibole are not frequently in contact, the trace element signature of amphibole cannot originate by subsolidus reaction with diopside. It follows that the trace element contents of clinopyroxenes of the peridotites result from equilibrium with a melt rich in the most incompatible elements except Ta and Nb. Otherwise, as interstitial amphibole and clinopyroxene have similar REE patterns (with similar partition coefficients for REE; Table 4) and are both relatively poor in Rb, K, Nb (no Ta data for amphibole), Zr, Ti, Fe and Al, but relatively rich in Mg and Cr, as they also have the same habit and occupy the same types of site in the peridotites, it is logical to assume that both were neoformed by reaction of the same melt with olivine, enstatite and spinel. Group I peridotites are thus secondary lherzolites. Considering now the amphibole veins and clinopyroxenites (group II), the chemical compositions suggest that the monomineral veins were the result of an intensive metasomatism of secondary lherzolites by a melt rich in all of the most incompatible elements. Olivine in clinopyroxenites, and clinopyroxene and olivine in amphibole veins can be considered as partially resorbed phases of previously metasomatized peridotites.

Chronology of events

The question rises now of knowing if these metasomatic events were due either to only one melt which would differentiate during a process of percolation either from veins towards the surrounding peridotites (hypothesis 1) or the reverse (hypothesis 2), or to different melts during two successive events (I then II) of percolation (hypothesis 3). This third hypothesis appears the best constrained from physical and chemical points of view. Indeed, the field experience shows in general that, when there is an infiltration along a fracture, there is first crystallization at the edges, thus formation of a rim, and then crystallization progresses inwards. An impregnation of the surrounding rock can occur but on a limited distance and anyhow during the *initial* stage of the percolation. So it is ruled out that the interstitial amphiboles and clinopyroxenes have been formed after the amphibole of veins and the hypothesis 1 is unclaimed. The opposite physical process is easier to conceive, with first an infiltration of the rock along grain boundaries, then a collection and a draining along large fractures of the melt which has not been "adsorbed by metasomatic reactions" in the surrounding rock. However the petrographic observations of Vaselli et al. (1995) on these xenoliths, and also by Kempton (1987), Witt and Seck (1989), Witt-Eickschen et al. (1993) and Witt-Eickschen (1993) on a larger sampling of xenoliths show that the veins always crosscut the surrounding rocks and structures of collection are never observed. This last group of authors concluded in favour of two distinct and successive events of infiltration, first along grain boundaries, then along fractures. In our study the most incompatible trace element compositions of amphibole and clinopyroxene in both types of lithologies and the values of their partition coefficients for these elements (Table 4) definitively rules out hypothesis 2. Indeed these partition coefficients are all below 1 with $D_{Th} < D_{Ta} < D_{LREE} < D_{HREE}$. That implies that during a percolation process from peridotites towards the veins, the Th/Ta ratio (or Th/LREE or Th/HREE), and the Ta/LREE ratio (or Ta/HREE), of the percolating melt will increase together, whereas they evolve in opposite senses from the melt I to the melt II (see "Characterization of melts I and II" and Table 5). Let us remark that the chemical composition of clinopyroxenes and amphiboles indicates that porphyroclastic and IT granoblastic lherzolites are type I mantle lithologies (terminology of Frey and Prinz 1978), while clinopyroxenites, amphibole clinopyroxenites and veins are type II. The HT granoblastic facies are hybrid and cannot be classified. As demonstrated by Kempton (1987), the type II lithologies always postdate the type I lithologies.

Evolution of the mantle chemical composition with successive metasomatisms

Correlation trends between major elements of whole rocks (Fig. 5 and in Vaselli et al. 1995), which are considered as tracers of melting processes in peridotites, are also tracers of mixing processes between mantle and two

Table 5 Calculated trace element compositions of liquids in equilibrium (1) with metasomatic clinopyroxenes in secondary lherzolites (MELT I) and in clinopyroxenites (MELTS II for BG00 and Bgt16); (2) with metasomatic amphiboles in amphibole veins (MELTS II for Lgf11 and BC01). Trace element compositions of some representative samples of melilitites (Wilson et al. 1995), melanephelinites (STK210 and P423 from the Pannonian Basin, in Embey-Istzin et al. 1993; TL944 and TL973, in Simonetti and Bell 1994) and magnesian leucitites (Rogers et al. 1985) are shown for comparisons

	Melts I						Melts II				Melilitites				Mela-nephelinites				Mg-leucitites
	BG-04	BG-10	BG-15	BgT6	BgT7	BgT21	BG-00	BgT16	Lgf11	BC 01	U9	U2	RH1	H9	STK210	P423	TL944	TL973	
Rb	167	196	204	188	97	151	182	97	35	29	42	64	42	52	105	33			396
Ba	588	821	971	499	611	928	2149	1674	1108	1084	1445	1257	997	1087	1658	665	1180	888	738
Th	42	21	14	73	205	53	14	18	34	34	8	15	13	17	19	11			30
Ta	1.30	1.39	0.57	1.77	1.31	1.99	8.37	15.60	30.02	12.91									0.6
Nb	14	20	7	15	26	33	115	160	754	323	137	121	116	131	147	117	110	55	7
La	26	9	8	23	41	37	31	48	186	78	94	84	83	89	127	87			52
Ce	50	26	22	37	58	57	71	107	346	168	172	148	151	166	243	198			124
Pb	31	33	64	35	73	52	25	39	114	61	4	4		5	7	7			
Sr	809	648	486	620	752	1046	792	1219	1424	1515	1390	1071	1286	1267	1736	1256	1188	415	791
Nd	22	16	16	19	21	20	34	51	115	73	72	58	66	68	86	87	157	87	56
Zr	295	237	241	274	314	186	227	384	790	759	301	224	285	277	366	504			182
Hf	4.0	3.3	3.6	3.5	4.0	2.3	4.1	6.5	7.4	7.8									5.0
Sm	5.7	5.0	5.0	5.5	5.7	5.1	8.0	11.6	19.4	14.3	12.2	9.4	11.6	11.4					11.0
Eu	2.0	1.9	1.8	1.9	2.0	1.7	2.4	3.5	5.6	4.1	3.4	2.7	3.2	3.2					2.3
Ti	7339	7183	5621	5777	4528	5777	13897	19518	21743	25088	15769	15230	15530	17209	12112	23864	16249	15110	4497
Gd	5.7	5.7	5.5	6.0	6.4	5.3	6.6	10.3	10.3	7.5	9.2	7.0	9.6	8.9					8.8
Tb	1.1	1.1	1.1	1.0	1.2	1.0	1.2	1.6	2.0	1.5									1.3
Dy	7.2	7.5	7.5	7.2	7.8	6.9	7.0	9.1	10.5	8.3	6.2	4.4	7.4	6.4					
Er	4.6	4.8	4.9	4.7	5.3	4.8	3.7	4.8	6.2	4.6	2.5	1.8	3.7	2.7					
Yb	4.0	4.5	4.6	4.2	4.9	4.4	2.9	3.9	8.1	6.1	1.8	1.3	3.0	2.1				1.8	
Lu	0.6	0.7	0.7	0.8	0.8	0.7	0.5	0.6	0.8	0.6	0.3	0.2	0.3						
Ba/Nb	43	42	145	33	23	28	19	10	1	3	11	10	9	8	11	6	11	16	105
Th/Nb	3.1	1.0	2.1	4.8	7.9	1.6	0.12	0.11	0.04	0.11	0.06	0.12	0.11	0.13	0.13	0.09			4.3
La/Nb	1.9	0.5	1.2	1.5	1.6	1.1	0.27	0.30	0.25	0.24	0.68	0.69	0.71	0.68	0.86	0.74			7.4
La/Yb	6.5	2.0	1.8	5.5	8.4	8.4	10.4	12.3	22.9	12.7	51.2	62.9	27.9	42.9					28.6
Sr/Nb	59	33	73	40	29	32	7	8	2	5	10	9	11	10	12	11	11	8	113
Zr/Nb	22	12	36	18	12	6	2.0	2.4	1.0	2.3	2.2	1.9	2.5	2.1	2.5	4.3	1.4	1.6	26
Sr/Zr	2.7	2.7	2.0	2.3	2.4	5.6	3.5	3.2	1.8	2.0	4.6	4.8	4.5	4.6	4.7	2.5	7.6	4.8	4.3
Sr/Yb	204	145	105	147	155	237	271	315	175	248	760	805	434	612					437
Zr/Yb	74	53	52	65	65	42	78	99	97	124	164	168	96	134					101
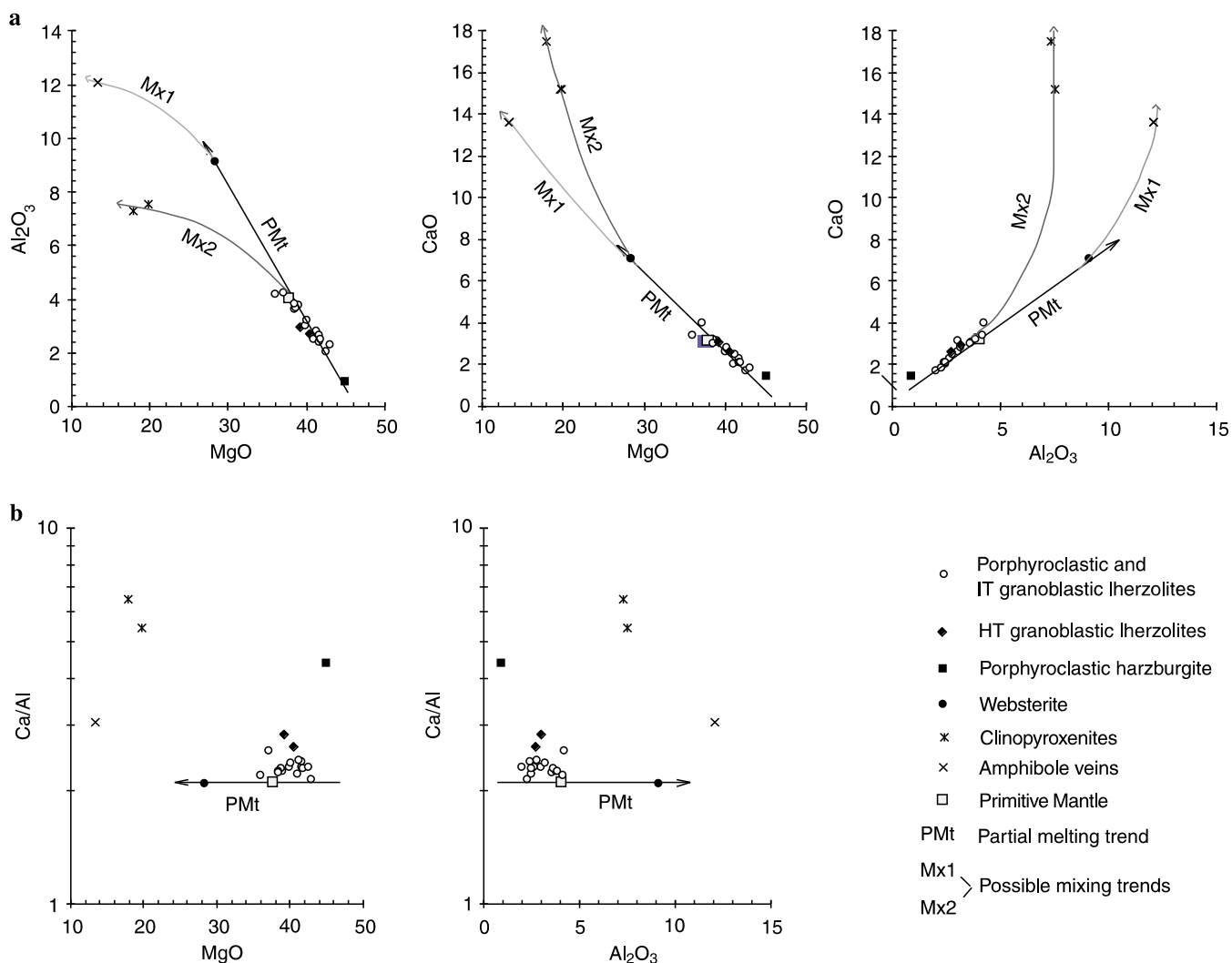
Fig. 5a,b Correlations on whole rocks of peridotites and veins: **a** between MgO, Al₂O₃ and CaO in order to visualize the superimposition of possible melting (*PMt*) and mixing (*Mx*) trends; **b** between Ca/Al, MgO and Al₂O₃ in order to visualize the slight and variable Ca-enrichment of most of the peridotites; data on the primitive mantle from Hofmann (1988)

distinct melts (I and II), unless it transpires that the mixing trends are more extended and diversified than melting trends. Indeed the former are controlled, not only by the composition and the proportion of both mixing end-members (mantle and contaminant melt), but also by the partition coefficients for major elements of primary phases in resorption and metasomatic phases in neoformation. This is visualized in major element variation diagrams (Fig. 6 in Vaselli et al., 1995 and Fig. 5 in this paper) by the different shapes of compositional trends of the websterite and veins. In contrast the compositional trends of secondary lherzolites superpose more or less on the assumed melting trend. This means that the major element composition of peridotites was not significantly modified by interstitial metasomatism. Nevertheless the Ca/Al ratio of these peridotites

(Fig. 5) is often slightly higher (up to 2.9 for peridotites, 4.4 for the harzburgite) than that of the PM (2.2; Sun 1982) and is rather variable. This suggests an enrichment in Ca relative to Al in these rocks and confirms that at least the Al content of lherzolitic and harzburgitic whole rocks has not been significantly modified by metasomatism and can be considered as a tracer of the initial state of depletion of the mantle.

The correlations between Al₂O₃ and some trace elements in whole rocks enable further to decipher the evolution of trace element compositions of peridotites by metasomatism. Whole-rock Al₂O₃ has been plotted against whole-rock Th, Ta, La and Sm contents which are respectively representative of LFS (low field strength), HFS (high field strength), LRE and MRE elements (Fig. 6). Good correlations between Al₂O₃ and Sm, and to a lesser extent (due to the very low concentrations) Ta, exist from the harzburgite through the porphyroclastic and I*T* granoblastic lherzolites to the websterite, while there is a scattering of data when Al₂O₃ is plotted against Th or La. This indicates that Ta and Sm can be considered as tracers of the composition of

Fig. 6a–d Chemical data plots of whole rocks from harzburgite (*black square*), websterite (*black circle*), porphyroclastic and I*T* granoblastic lherzolites (*white circles*), H*T* granoblastic lherzolites (*black diamonds*) and clinopyroxenites (*stars*): **a** Al_2O_3 versus Ta; **b** Al_2O_3 versus Sm; **c** Al_2O_3 versus Th; **d** Al_2O_3 versus La. Whole-rock data from amphibole pyroxenites are not displayed here because they plot outside of all the diagrams
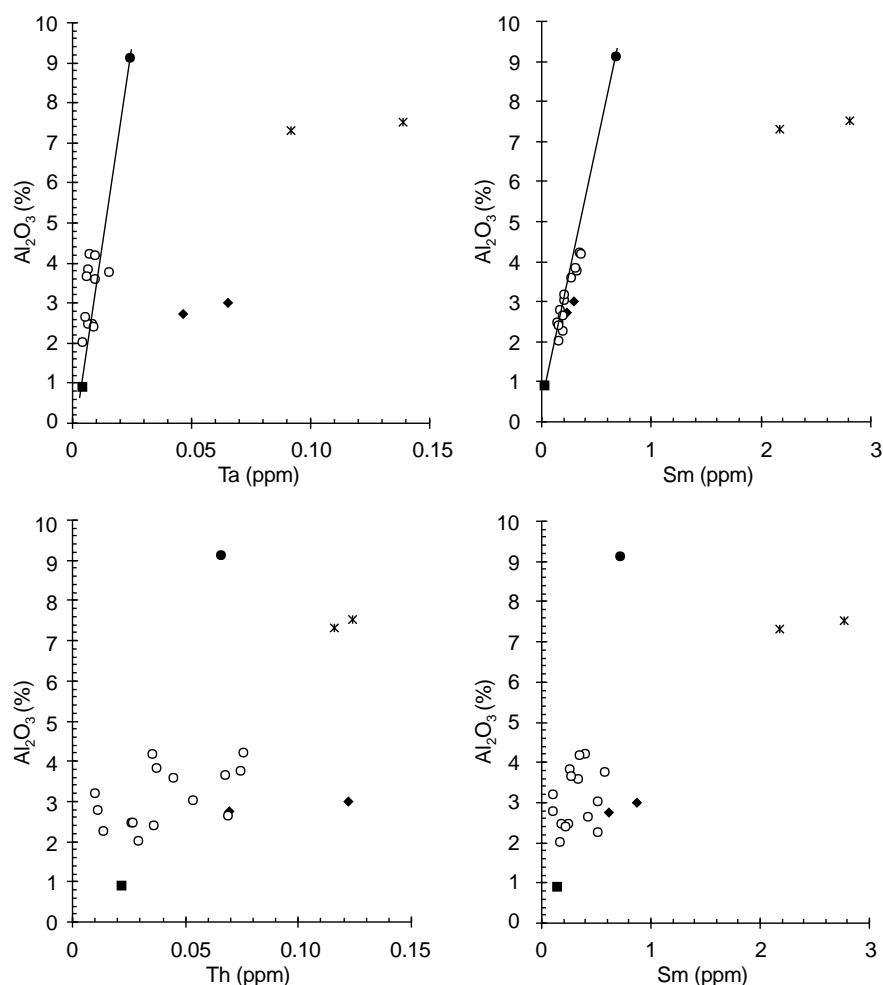
the mantle before metasomatism because they were not modified by metasomatism, nor by the late-stage phases in microfractures (Chalot-Prat et al. 1995). On the other hand Th and La can be considered as tracers of the extent of metasomatism. The low Ta and Sm contents of these lherzolites indicate that the initial mantle was rather depleted in incompatible elements relative to the PM and was thus to some extent residual. This further indicates that metasomatism probably involved a very small fraction (<1%) of a relatively Ta- and Sm-poor but Th-, U- and also relatively LREE-rich melt. With the lowest Ta and Sm contents, the harzburgite would result from a slight metasomatism of a highly depleted mantle. With the highest Ta and Sm contents (Sm being even higher than in PM) and a pattern which remains LREE-depleted, the reconstituted pattern of the websterite before the metasomatic event is that of a typical N("normal")-MORB. Thus the websterite would result from the slight metasomatism of a partial melting product of a depleted mantle. The fact that its Ca/Al ratio remained equal to that of PM (Fig. 5) supports this hypothesis, the metasomatism being slight enough not to modify significantly the already high contents in CaO of the premetasomatic rock.

In the H*T* granoblastic lherzolites, only Sm correlates with Al_2O_3 while Ta is higher than expected, suggesting a metasomatism by a relatively Ta-rich but Sm-poor melt. Thus this facies could result from two successive metasomatisms, first Ta-poor, then Ta-rich, which would account for the hybrid signature of the clinopyroxenes. The whole-rock Ca/Al ratios are higher (2.6–2.9) than those of the porphyroclastic facies, which confirms the further enrichment indicated by trace elements. This is also consistent with the larger size of clinopyroxenes.

Clinopyroxenites, amphibole veins and amphibole pyroxenites are enriched in Th, Ta, La and Sm relative to all the other rocks, suggesting a strong metasomatism by a Ta-rich melt. The signature of clinopyroxenes of amphibole pyroxenites suggests, as in the H*T* granoblastic facies, that the mantle was twice metasomatized, but that the involved fraction of the Ta-rich metasomatic melt was much higher than in the granoblastic facies. The Ca/Al ratios of veins are relatively high (3 for amphibole pyroxenite Lgf11; 5.5 and 6.5 for clinopyroxenites) compared to the PM, and support the hypothesis of a metasomatism by a melt with a high Ca/Al ratio.

Summary

The porphyroclastic and IT granoblastic lherzolites were initially harzburgites to clinopyroxene-poor lherzolites. These underwent impregnation by a melt I which induced the formation of interstitial clinopyroxenes and amphiboles by metasomatism of host minerals. Percolation of the melt induced textural recovery. Harzburgite and websterite could be variations of these secondary lherzolites in which the melt infiltrated either more residual parts of the mantle or crystallized partial melting products. This attests that the relative heterogeneity of the original mantle was linked only to partial melting processes. Only a very small fraction of liquid I reacted with the original rock, and metasomatism did not significantly modify the major element composition of peridotites. The HT granoblastic lherzolites were also initially harzburgites to clinopyroxene-poor lherzolites which would have thus undergone two successive metasomatic events. Amphibole clinopyroxenites and amphibole veins are genetically linked and the amphibole clinopyroxenites would represent a transitional facies between the secondary lherzolites and the amphibole veins. These latter are totally transformed parts of the mantle outlining fracture zones percolated by an H$_2$O-rich melt. Clinopyroxenites are, in contrast, parts of the mantle almost completely transformed by percolation of an H$_2$O-poor melt. The "hybrid" characteristics of clinopyroxene from HT granoblastic lherzolites could indicate that this facies was a transitional facies between secondary lherzolites and clinopyroxenite veins.

Fig. 7a,b PM-normalized spidergrams of calculated trace element compositions of contaminant melts: **a** melts I in equilibrium with clinopyroxenes of secondary lherzolites (websterite included) and harzburgite (*large black square*); **b** melts II in equilibrium with amphiboles of amphibole pyroxenites (Lgf 11: *black square*; BC 05: *star*) and veins (BC 01: *black triangle*), or in equilibrium with clinopyroxenes of clinopyroxenites (BG00: *black circle*; Bgt16: *black diamond*). The hybrid features of melts calculated from clinopyroxenes of amphibole pyroxenite (BC O5: *white triangle*) and HT granoblastic lherzolites (BG02: *white circle*; BG18: *white diamonds*)

Characterization of melts I and II

Major elements

It has been recognized by Meen (1987), Green and Wallace (1988) and Falloon and Green (1990) that metasomatism by Ca-rich silicate and/or carbonate melts leads to the neoformation, from original mantle minerals, of clinopyroxenes and/or amphiboles depending on the CO$_2$/H$_2$O ratio of the melts. If clinopyroxene was initially present, its size must increase at the expense of other minerals. Olivine and orthopyroxene progressively disappear as assimilation of melt by the mantle rock increases. Based on these results, the petrographic observations of Persani Mts xenoliths suggest a two-stage metasomatism by Ca-rich carbonated and/or silicated melts. Indeed in the peridotites and veins, not only do clinopyroxene and amphibole show habits and textural relationships of metasomatic minerals but olivine is never neoformed and displays, in the veins, the habit of a mineral previously deformed and in process of resorption. As shown by contrasted clinopyroxene and amphibole compositions in interstitial and vein locations, the successive melts differed in their relative proportions in some major elements: melt I was richer in Mg and Cr, similar in Na but poorer in Ti, Fe, Al and K than melt II. These Ca-rich melts have a significant but limited alkaline content with a Na$_2$O/K$_2$O ratio higher than 1. Furthermore the formation of both types of veins required melts II with contrasted CO$_2$/H$_2$O ratio (Meen 1987; Green and Wallace 1988).

Trace elements

The trace element composition (including Ti) of these melts I and II can be obtained using known partition coefficients (Table 4) of trace elements for mantle clinopyroxenes and amphiboles, providing that the trace element contents of host-mantle minerals which reacted with the melt are negligible compared to those of the

melt. This is verified in both cases. In peridotites, as previously noted, mass balance calculations between whole-rocks and diospside (and amphibole) attest for a negligible content in trace elements of other minerals. This is less obvious—a priori—for amphiboles in clinopyroxenites and veins since they crystallized in an already metasomatized mantle in which metasomatic clinopyroxenes were in variable proportions. As the patterns of amphiboles in veins and clinopyroxenites strictly agree, their composition is believed to be mainly influenced by this of the melt II. The same conclusions can be reached concerning the composition of the liquid calculated from clinopyroxenes of clinopyroxenites.

The trace element composition of the contaminant liquids is calculated as follows:

a. From clinopyroxenes (Table 4) using: (1) average $D^{cpx/melt}$ for most elements from the literature (in Chazot et al. 1996) which are in good agreement with the measured values in natural lherzolites (Chazot et al. 1996) and those obtained by experimentation on REE and some other elements (Hart and Dunn 1993); (2) $D^{cpx/melt}$ for K and Ti from the experimental results of Hart and Dunn (1993); (3) $D^{cpx/melt}$ for Ta estimated from average $D^{cpx/melt}$ for Th, knowing that in clinopyroxenes D_{Th} is always slightly lower or equal to D_{Ta} (with $D_{Th}/D_{Ta} = 0.6$ on average) (Irving and Frey 1984; Lemarchand et al. 1987).

b. From amphiboles (Table 4) using: (1) $D^{amp/melt}$ for Th, Sr and REE from data on JK2 sample in Chazot et al. (1996); (2) $D^{amp/melt}$ for HFSE, Rb, Ba and K from the experimental results of Dalpé and Baker (1994). The D values for REE given by Dalpé and Baker (1994) are not far from those measured by Chazot et al. (1996) but are too low to fit with the results $D^{amp}/D^{cpx} = 1.1$ obtained by Chazot et al. (1996) with in situ analyses in the same mantle rock.

These D values are those of clinopyroxene and amphibole crystallized in a basaltic melt at mantle pressures. They are slightly lower for clinopyroxene and much lower for amphibole than those given by Irving and Frey (1984), used by Vaselli et al. (1995) and which reflect element partition between minerals and a basaltic magma rising to the surface. This difference of D values causes an important change in the calculated composition of the contaminant melts. Two additional problems exist: (1) K_2O content calculated from clinopyroxenes is systematically higher than that obtained from amphibole from the same rock. This could be due to poor precision on the low K_2O content of the clinopyroxenes. So only the K_2O content derived from amphibole will be taken into account in the discussion of the results and the K content of melts I and II has not been reported on trace element diagrams; (2) in the peridotites, the TiO_2 content calculated from clinopyroxenes is always lower than that obtained from amphiboles in the same rock. Since the TiO_2 contents of clinopyroxenes and amphiboles are always above the detection limit by microprobe, this difference could only be due to minor inconsistencies in the chosen partition coefficients. In any case these slight variations have no effect on the interpretation of the results since amphiboles and pyroxenes always have much higher TiO_2 contents in pyroxenites and veins than in peridotites.

The melts I and II (Table 5) are characterized by very high trace element contents (10 to 800 times PM) (Fig. 7a, 7b) and show marked positive anomalies in Rb, Ba, Th, Sr and Zr. Melt I differs from melt II in having much lower Ta and Nb contents, thus much higher Th/Ta_N, lower LREE contents and LREE/HREE ratios, and in being much less titaniferous and potassic. Besides the liquids in equilibrium with clinopyroxenes of HT granoblastic lherzolites and clinopyroxenites (Fig. 7b) are rather similar, except the former are poorer in TiO_2 and LREE, which supports the hypothesis that the HT granoblastic lithology was twice metasomatized. The liquid in equilibrium with the clinopyroxenes of the harzburgite (Fig. 7a) has the particularity of being very poor in MREE and HREE. It could be a residual liquid of melt I and this harzburgite would thus represent a distal facies relative to the porphyroclastic lherzolites. On the whole the low fractionation of REE in melt I, the interaction of a very small fraction of this melt with the depleted mantle and the low partition coefficients of clinopyroxenes and amphiboles for the LREE, can explain why both of these metasomatic minerals mostly display LREE-depleted spidergrams. The melts II involved in the formation of amphibole veins and clinopyroxenites have very similar patterns, except that the former is generally more enriched in all trace elements. This could be the result of different degrees of melting of the same source, the CO_2/H_2O ratio increasing as the degree of melting increases (see "Possible source-rocks...").
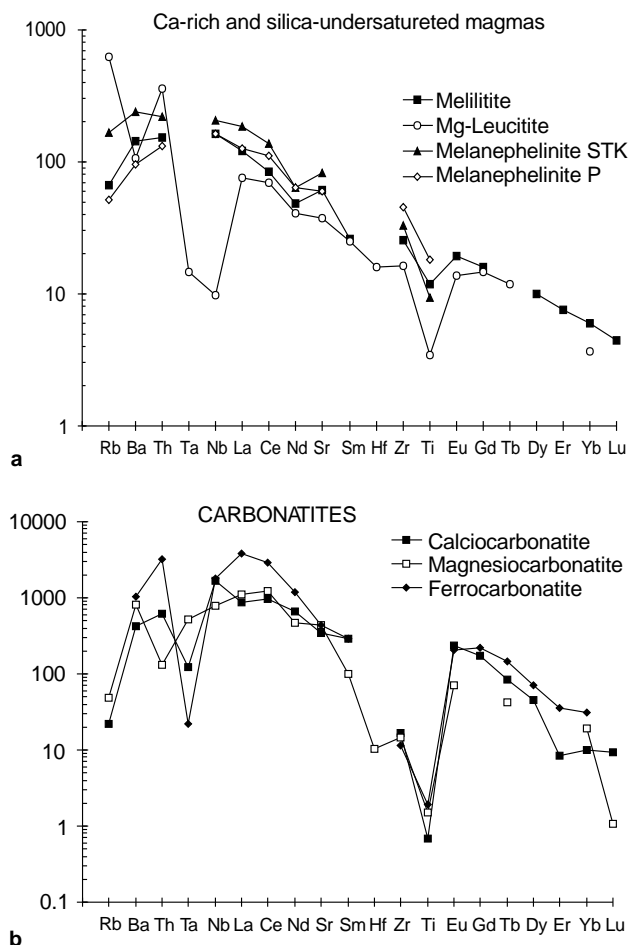
Fig. 8a,b For comparison with trace element compositions of melts I and II, trace element spidergrams of: **a** representative samples of Ca-rich and highly silica undersaturated magmas (melilitite data in Wilson et al. 1995; Mg-leucitite data in Rogers et al. 1985), **b** the 3 types of carbonatitic facies (average data from Woolley and Kempe 1989)

Comparisons with other magmas: melt I = melilitites and melt II = melanephelinites

Based on the previously mentioned experimental studies, the melts I and II can be analogous either to highly silica-undersaturated ultrabasic magmas (data in Le Bas 1989; Embey-Istzin et al. 1993; Simonetti and Bell 1994; Wilson et al. 1995) or to carbonatites (data in Woolley and Kempe 1989). As demonstrated above, the major element compositions of the highly undersaturated silicate magmas are believed to be close to those assumed for melts I and II. The carbonatites have compositions that are too contrasting and too poor in alkaline elements. Furthermore the silicate magmas have a compositional diversity that appears well adapted to the differences existing between melts I and II. Indeed both these melts can easily be compared to the most mafic, silica-undersaturated and sodic members of the alkali basalt series, respectively melilitites and melanephelinites (Table 5 and Fig. 8). These rocks are poor in SiO_2 (<40% in melilitites; <44% in melanephelinites) and Al_2O_3 (<11% in melilitites; <13% in melanephelinites), very rich in CaO (11–18%) and MgO (14–19% in melilitites; 8–13% in melanephelinites), and have a limited total alkali content (Na_2O: 1–3% in melilitites and 3–7% in melanephelinites; K_2O: 0.5–2.5% in melilitites and 1.5–3.5% in melanephelinites) with $Na_2O \gg K_2O$. However their somewhat high TiO_2 content(2.5–4%) and their trace element ratios and contents (Table 5) agree only with those of melts II, unless the REE spidergrams of these ultrabasic lavas are much more fractionated than those of melts II. Surprisingly, only the magnesian leucitites (lamproïtes of Type III in Wilson, 1989; data from Rogers et al., 1985), which are potassic equivalents of melilitites and melanephelinites but poorer in TiO_2 (0.6%), show a trace element distribution close to that of melt I (Table 5) with specifically low Ta and Nb contents. It is however precluded that melt I was potassic. All these points of similarity or dissimilarity can be explained when considering the possible genetic relationships between melts I and II and the mineral phases responsible for controlling element partioning in the source (see following section).

Possible source-rocks for melts I and II

Major and trace element constraints

By considering the variations of major and trace element contents from melt I to melt II, it is possible to decipher their relationships and to estimate the mineralogy of their sources. However these variations cannot be correlated in an easy way, i.e. assuming that both major and trace element contents of melts are controlled only by the fusible or refractory behaviour of major phases in the source. All is much clearer if major and minor phases of the source are assumed respectively to control major and trace element composition of the melt. This leads to

the hypothesis that melts I then II were extracted during a two-stage partial melting from the same source, at high pressure and under increasing temperature conditions as suggested by the previously mentioned experimental results. The source rock should include at least garnet, amphibole, clinopyroxene and calcite or dolomite. Indeed in a first approach, the contrasting contents of melts I and II in Mg and Cr on one hand, and in Ti, Fe, Al and K (even if K content remains low) on the other hand, could be explained by melting of garnet (Cr-rich pyrope variety ?) during the first stage, while both other silicate phases remained rather refractory; during the second stage amphibole and/or clinopyroxene melted in turn giving variously H_2O-enriched melts. This scenario agrees with experimental results in hydrous conditions of Hellman and Green (1979). Pyrope garnet might be a hydrogarnet as observed in a number of mantle as well as granulite facies rocks (Aines and Rossman 1984a, b) and thus the main H_2O source in melt I as suggested by these last authors and Geiger et al. (1991). Calcium is an important constituent of all of these silicate phases. Based on numerous experimental results (references in Pyle and Haggerty 1994; Falloon and Green 1994), the Ca content of the melts was likely controlled by a Ca-rich carbonate. All of these phases characterize HT-HP lithologies, i.e. a carbonated metasomatized mantle or eclogites either of mantle (Pyle and Haggerty 1994, and references therein) or crustal (Newton 1986) affinity. The same reasoning can be used with trace elements, providing that they were controlled by various accessory phases during melting, even if major phases cannot be excluded for some elements. Indeed minor phases are well known for having much higher trace element contents and much more selective partition coefficients from one to another element than major phases. In addition all of the minor phases mentioned below are known in metasomatized mantle facies (Haggerty et al. 1983; Erlank et al. 1987; Lloyd 1987; Yaxley et al. 1991; Ionov
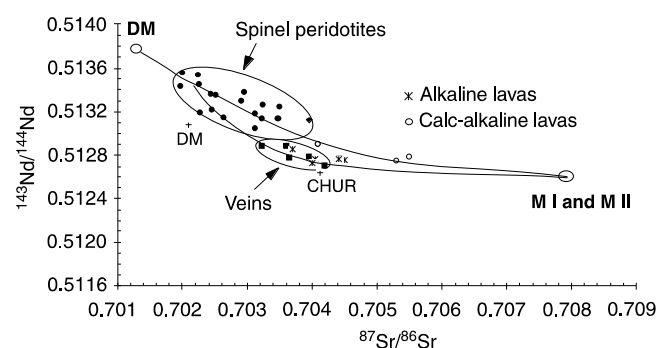
Fig. 9 Distribution of Nd and Sr isotopic data of separate clinopyroxenes and amphiboles from spinel peridotite and xenoliths veins (Vaselli et al. 1995), and of the most primitive alkaline (Downes et al. 1995) and calc-alkaline (Mason et al. 1996) lavas from Romania, and for the modelling of hypothetical successive mixing induced by metasomatism of the mantle between mantle end-members [depleted mantle (DM) or spinel lherzolites] and contaminant melts (M I and M II)

et al. 1993; Rudnick et al. 1993; McInnes and Cameron 1994; Chalot-Prat et al. 1995; Gebauer 1995), but also indeed in continental crustal mafic facies (Sobolev and Shatsky 1990; Rudnick 1992). Thus in the present study, REE fractionation but also Th, U and even Sr contents of melts can be controlled by the melting of apatite and/or monazite (Henderson 1984; Nriagu and Moore 1984), which may partly be counterbalanced by melting of zircon, itself traced by high enrichments of the melt in U, Zr and Hf, and a relative enrichment in HREE (ICP-MS data). The LREE/MREE ratio can also be attenuated by melting of sphene, which is traced by high enrichments in Ta, Nb and MREE, but also in Ti, in the melt (Hellman and Green 1979; Wörner et al. 1983). On the other hand enrichment in Ta, Nb and Ti relative to Th, U and REE, without any modification of REE fractionation, can characterize melting of rutile (Brenan et al. 1994). The Rb, Ba and Sr, and at least in part K, Na and Ca , can be controlled by Ba and K end-members of a Ti-oxide series (only observed until now in kimberlites and veined peridotites after Haggerty et al., 1983). This list of minerals and the types of possible combinations that depend first on the fusible or refractory behaviour of co-existing phases, is far from being inclusive, so a simple scenario cannot at present be proposed. Nevertheless the trace element pattern of melt I was not controlled by exactly the same phases as that of melt II. For example the difference in REE fractionation between melts I and II could result from the melting of apatite associated only in the first stage with that of zircon; in the same way the contrasted contents in Ta, Nb and Ti of both melts could be attributed to the refractory then fusible behaviour of rutile and/or sphene during the two-stage melting. Moreover the solubility of zircon during melting of basic rocks increases with the peralkaline character of the extracted melt (Watson and Harrison 1983), which could be the case for melt I, which is much less aluminous than melt II. Based on this reasoning, element partitioning is believed to have been controlled by the same association of accessory phases in the sources of melt I and magnesian leucitites on one hand, and of melt II and sodic melanephelinites on the other hand. The higher HREE contents in melt I (4–5 ppm Yb) and II (3–8 ppm Yb) than in the analogous magmas (1–2 ppm Yb) could reflect the major roles of zircon followed by sphene during genesis of contaminant melts.

Nd and Sr isotopic constraints

The Nd and Sr isotopic data on separate clinopyroxenes and amphiboles of peridotites and veins (Vaselli et al. 1995) confirm the previous results, namely that the source of contaminant melts belong to either an already metasomatized subcrustal mantle or a basic lower crust. Indeed, these Nd and Sr isotopic ratios lie in the depleted mantle field of the Nd-Sr isotope diagram (Fig. 8a in Vaselli et al., 1995; Fig. 9 this paper). Considering that all these minerals are metasomatic, these data can

Table 6 Trace element compositions (ppm) of the most primitive calc-alkaline lavas from the East Carpathians

| | RUP | PM-C1 | PM-C4 | PM-H11 |
	a	b	b	b
%SiO$_2$	54.5	52.2	51.2	54.9
Ba	286	370	134	489
Ce	38.34	47.63	16.11	32.17
Co	74.87	63.34	38.67	46.95
Cr	72.89	190.36	21.72	47.34
Cs	0.192	3.109	0.559	1.845
Dy	2.95	4.53	3.75	3.60
Er	1.51	2.49	2.15	2.20
Eu	1.354	1.330	1.051	1.226
Ga	22.19	20.49	18.60	20.89
Gd	3.53	4.92	3.12	3.24
Hf	3.05	4.41	1.88	2.72
Ho	0.621	1.010	0.818	0.813
La	19.49	22.26	7.07	18.01
Lu	0.248	0.465	0.335	0.335
Nb	9.98	8.67	2.89	10.40
Nd	19.49	25.10	11.50	16.05
Ni	37.14	66.20	10.79	19.92
Pb	4.89	17.36	6.30	22.44
Pr	4.67	6.04	2.34	3.87
Rb	17.37	75.08	21.22	36.95
Sm	4.21	5.92	2.87	3.67
Sr	653	250	272	937
Ta	1.27	0.98	0.42	0.96
Tb	0.564	0.834	0.602	0.565
Th	4.05	7.68	1.46	4.38
Tm	0.261	0.406	0.325	0.329
U	0.882	2.372	0.639	1.551
V	117	238	322	213
Y	16.52	27.07	21.28	22.71
Yb	1.39	2.60	1.99	2.02
Zr	139	181	75	110

[a] %SiO$_2$ from Downes et al. (1995)
[b] %SiO$_2$ from Mason et al. (1996)

be interpreted in terms of mixing between a depleted mantle (DM: initial depleted mantle; SP: spinel peridotite) and 2 liquids (M I and M II) which could have the same isotopic signature at the limit between mantle and crust fields. Mixing hyperbolas have been hand-drawn on Fig. 9 knowing that: (1) the convexity of mixing hyperbolas depends on both the Nd content (C_{Nd}) of each end-member and the value of the ratio $C_{Nd(mantle)}/C_{Nd(melt)}$ (cf. Faure 1986, for theory); after our calculations (Table 5) and those of Hoffman (1988) on trace element contents of a depleted mantle, $C_{Nd(M.II)} > C_{Nd(M.I)}$, $C_{Nd(DM)}/C_{Nd(M I)} < 1$ and $C_{Nd(SP)}/C_{Nd(L II)} \ll 1$, which leads to an hyperbola SP - M II more convex than the hyperbola DM - M I; (2) the proportion of each end-member in the mixture is controlled by the percentage of the neoformed metasomatic minerals in the mantle and their partition coefficients; this percentage is much lower in peridotites than in veins. These constraints lead to the assumption that the isotopic signature of the source of contaminant melts lies somewhere in a site where it is common also to find isotopic signatures of enriched or metasomatized mantle as well as of continental crust (see data compilation in Wilson, 1989).
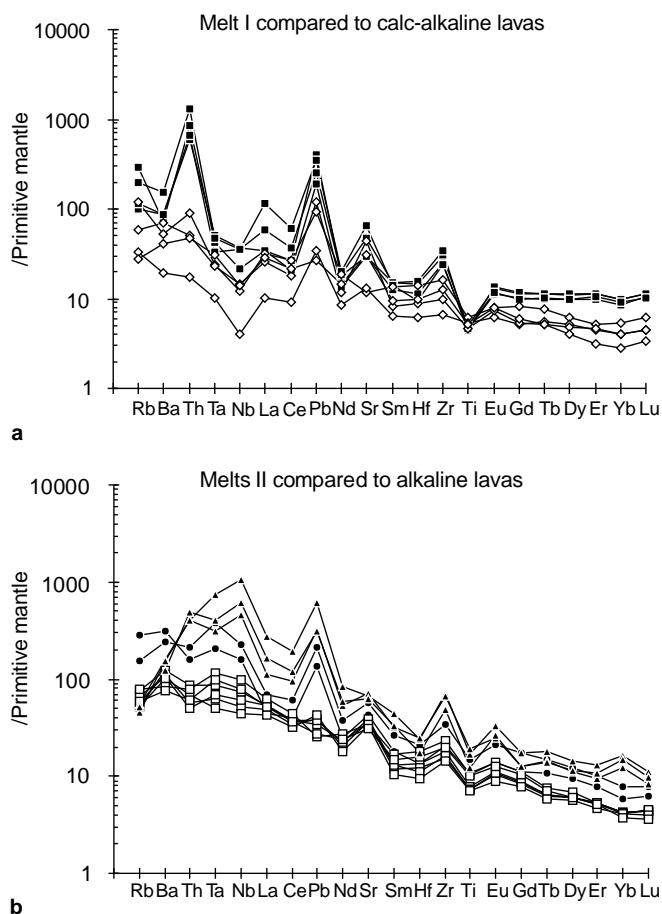
Fig. 10a,b Comparison of trace element diagrams of contaminant melts with the most primitive recent lavas of the Eastern Transylvanian Basin of Romania: **a** melt I (*black squares*) with calc-alkaline lavas (*white diamonds*); **b** melts II (from amphibole veins *black triangles*, from clinopyroxenites *black circles*) with alkaline lavas (*white squares*)

Summary

Constraints brought by major and trace elements and Nd and Sr isotopic signatures suggest that source rocks of melts I and II equilibrated at H*T*-H*P* either in a strongly metasomatized sub-crustal mantle (Falloon and Green 1990) or in a metamorphic basic crust. Pyle and Haggerty (1994) demonstrated that eclogites could be good candidates as possible sources of highly undersaturated primitive melts. This raises the question of whether eclogites formed part of an oceanic or continental slab subducted into the lithospheric mantle of Romania. The likely involvement, during melting, of specifically U-enriched phases, is in favour of eclogites enclosed in a deep and polymetamorphic continental crust. The presumed shallow depth of the metasomatized mantle of Romania (Vaselli et al. 1995), not far from the crust-mantle interface, fits also better with eclogites of continental affinity. In that case, melting of eclogites could have occurred by delamination and suboverthrusting of lower crust into the mantle during a previous orogenesis. This possibility fits (1) with the

conclusions of Wilson and Downes (1992) according to which the composition of the lithospheric mantle is to some extent constrained by its previous orogenic history; (2) with the structural and tomographic studies of Wenzel (1997) emphasizing the major role of plate delamination into the mantle during the last 10 Ma, i.e. since active subduction has stopped.

Relationships between melts I, melts II, alkaline and calc-alkaline lavas in the persani mountains

Vaselli et al. (1995) assumed that the mantle metasomatism was related to the percolation of an alkaline basic magma with a composition close to that of the lavas which host mantle xenoliths in the Eastern Carpathians. Our study leads us to different conclusions. Indeed the inferred bulk compositions of melts I and II are clearly different from alkaline (Downes et al. 1995) and calc-alkaline basic lavas (Downes et al. 1995; Mason et al. 1996; Table 6): the relative proportion of major elements is not at all the same and their trace element contents relative to PM are much higher (Fig. 10). Nevertheless both contaminant melts show strong positive anomalies in Th, Sr and Zr, and a Ti negative anomaly, which are both present, although attenuated, in the patterns of the two types of lavas. In the same way melts I and calc-alkaline lavas on one hand, and melts II and the alkaline lavas on the other hand differ from each other by diametrically opposed Ta and Nb contents and different REE fractionation. So contaminant melts and basalts can be assumed to have only indirect relationships. A likely hypothesis may be that the lavas originated by melting of peridotites already metasomatized by melts I and II as previously envisaged by Wass and Rogers (1980) and Kempton (1987). This is supported by the similarity of isotopic ratios (Fig. 9) of alkaline lavas (Downes et al. 1995) and monomineral veins (Vaselli et al. 1995), and the fact that the isotopic ratios of the most primitive calc-alkaline lavas (Mason et al. 1996), although they differ from those of clinopyroxenes of peridotites, lie on the trend defined by the mixing hyperbola DM - M I. This would mean that the mantle source of calc-alkaline lavas was only more metasomatized by melt I than the mantle brought up as xenoliths by the alkaline lavas of Persani mountains. By this fact, the "calc-alkaline volcanic arc" could be linked to a continental delamination slab at the crust-mantle interface as proposed by Wenzel (1997). This hypothesis is an alternative to the conclusions of Mason et al. (1996) in favour of a contamination of the mantle source of calc-alkaline lavas by a subducted oceanic crust.

Conclusion

This study demonstrates that the shallow lithospheric mantle of the East Carpathians is the product of the

successive interaction of two different melts with an originally depleted mantle. The infiltration of a limited fraction of a melt I occurred along grain boundaries. It induced, by metasomatism, the appearance of interstitial clinopyroxenes and amphiboles and the formation of secondary lherzolites. Websterite and harzburgite are facies variations of this metasomatized heterogeneous mantle containing products (basaltic cumulates) and residues (harzburgites) of a previous partial melting event. Later large volumes of a melt II, at a higher temperature than melt I, percolated through fracture systems, induced a more or less complete resorption of the pre-existing minerals and the formation of clinopyroxene or amphibole veins, depending on the H_2O saturation of the liquid. Amphibole clinopyroxenites and some of the granoblastic lherzolites can be defined as proximal and distal facies of the secondary lherzolites relative to the veins. Correlation trends between major and trace element data in whole rocks show that the first metasomatic event slightly increased the Ca/Al ratio of the initial mantle without significantly modifying its major element bulk composition. The major element composition of veins is controlled by mixing between mantle and melt II and the type of metasomatic minerals which formed. Furthermore these correlations enable the importance and the number of metasomatic events undergone by each peridotite facies to be deciphered and confirm the strong depletion in the most incompatible trace elements and the residual state of the mantle before the first metasomatic event. Both the contaminant melts were Ca-rich and rather Si-poor, somewhat alkaline with Na_2O/K_2O higher than 1, while melt I differed from melt II by having systematically higher Mg and Cr contents and lower Ti, Fe, Al and K contents. Furthermore they were both highly enriched in all trace elements with strong positive anomalies in Rb, Ba, Th, Sr and Zr, but differed by their contrasting Ta, Nb and LREE contents, relatively lower in melt I than in melt II. They can easily be compared to highly silica undersaturated ultramafic magmas such as melilitites (melt I) and melanephelinites (melt II), except that melt I has trace element spidergrams closer to those of the potassic equivalents of these rocks, the magnesian leucitites. Such major and trace element distributions in each contaminant melt can be explained if they are assumed to be controlled respectively by major and accessory phases in the source during partial melting. Furthermore the recorded variations from melt I to melt II are explained when considering the behaviour, refractory or fusible, of these phases during a two-stage partial melting event of a single source. This source could be an already metasomatized mantle or more likely an eclogite, based on the natural genetic relationships observed between eclogite and silica-undersaturated liquids (Pyle and Haggerty 1994). Indeed the crustal affinity of the involved accessory phases would imply a deep crustal origin for these eclogites. Simple mixing modelling from the Nd and Sr isotopic data on the metasomatic minerals of peridotites and veins (Vaselli et al. 1995) does not enable a choice between both of these possibilities but supports the involvement of highly radiogenic components perhaps coming from the crust-mantle interface. Calc-alkaline and alkaline basic lavas of Romania have only indirect genetic relationships with the contaminant melts since the former could result from melting of the mantle metasomatized by melts I and II in a previous orogenic history.

This study of mantle xenoliths demonstrates that, when constrained by a detailed knowledge of relationships between deformation, recrystallization and metasomatic minerals in mantle rocks, the trace element composition of whole rocks and main trace element-bearing minerals provide a powerful tool for deciphering mantle evolution by melting and recycling processes.

References

Aines RD, Rossman GR (1984a) The hydrous component in garnets: pyralspites. Am Mineral 69: 1116–1126

Aines RD, Rossman GR (1984b) Water content of mantle garnets. Geology 12: 720–723

Bodinier JL, Vasseur G, Vernières J, Dupuy C, Fabries J (1990) Mechanisms of mantle metasomatism: geochemical evidence from the Lherz orogenic peridotite. J Petrol 31: 597–628

Brenan J, Shaw H, Phinney D, Ryerson F (1994) Rutile-aqueous fluid partitioning of Nb, Ta, Hf, Zr, U and Th: implications for high field strength element depletions in island-arc basalts. Earth Planet Sci Lett 128: 327–339

Carignan J, Machado N, Gariépy C (1995) U-Pb isotopic geochemistry of komatiites and pyroxenes from the southern Abitibi greenstone belt, Canada. Chem Geol 126: 17–27

Chalot-Prat F, Boullier AM, Arnold M (1995) Carbonatitic and silicated melts in a fissural network in mantle xenoliths from Romania: preliminary study with cathodoluminescence and electron probe. In: 2nd Int Workshop Orogenic Lherzolites, Granada (Spain), 24 August–5 September 1995, pp 9

Chazot G, Menzies MA, Harte B (1996) Determination of partition coefficients between apatite, clinopyroxene, amphibole and melt in natural spinel lherzolites from Yemen: implications for wet melting of the lithospheric mantle. Geochim Cosmochim Acta 60: 423–437

Dalpé C, Baker DR (1994) Partition coefficients for rare-earth elements between calcic amphibole and Ti-rich basanitic glass at

1.5 Gpa, 1100 °C. Goldschmidt Conf Edimburgh. Mineral Mag 58A: 207–208

Deer WA, Howie RA, Zussman J (1993) An introduction to the rock-forming minerals (2nd edn). Longman Scientific and Technical, Essex

Downes H, Seghedi I, Szakacs A, Dobosi G, James DE, Vaselli O, Rigby IJ, Ingram GA, Rex D, Pecskay Z (1995) Petrology and geochemistry of late Tertiary/Quaternary mafic alkaline volcanism in Romania, Lithos 35: 65–82

Embey-Isztin A, Downes H, James DE, Upton BGJ, Dobosi G, Ingram GA, Harmon RS, Sharbert HG (1993) The petrogenesis of pliocene alkaline volcanic rocks from the Pannonian Basin, Eastern Central Europe. J. Petrol. 34: 317–343

Erlank AJ, Waters FG, Hawkesworth CJ, Haggerty SE, Allsopp HL, Rickard RS, Menzies MA (1987) Evidence of mantle metasomatism in peridotite nodules from the Kimberley pipes, South Africa. In: Menzies MA, Hawkesworth CJ (eds) Mantle metasomatism. Academic Press Inc., London, pp 221–309

Falloon TJ, Green DH (1990) Solidus of carbonated fertile peridotite under fluid-saturated conditions. Geology 18: 195–199

Faure G (1986) Principles of isotope geology. John Wiley & Sons, New York, pp. 589p.

Frey FA, Prinz M (1978) Ultramafic inclusions from San Carlos, Arizona: petrologic and geochemical data bearing on their petrogenesis. Earth Planet. Sci. Lett. 38: 129–176

Gebauer D (1996) A P-T-t path for an (ultra?-) high pressure ultramafic/mafic rock-association and its felsic country-rocks based on SHRIMP-dating of magmatic and metamorphic zircon domains. Example: Alpe Arami (Central Swiss Alps). Earth Process: Reading the Isotopic Code, Geophysical Monograph 95: 307–329

Geiger CA, Langer K, Bell DR, Rossman GR, Winkler B (1991) The hydroxide component in synthetic pyrope. Am Mineral 76: 49–59

Green DH, Wallace ME (1988) Mantle metasomatism by ephemeral carbonatite melts. Nature 336: 459–461

Haggerty SE, Smyth JR, Erlank AJ, Rickard RS, Danchin RV (1983) Lindsleyite (Ba) and mathiasite (K): two new chromium-titanates in the crichtonite series from the upper mantle. Am Mineral 68: 494–505

Hart SR, Dunn T (1993) Experimental cpx/melt partitioning of 24 trace elements. Contrib: Mineral Petrol 113: 1–8

Harte B (1976) Rock nomenclature with particular relation to deformation and recrystallisation textures in olivine-bearing xenoliths. J Geol 85: 279–288

Hellman PL, Green TH (1979) The role of sphene as an accessory phase in the high-pressure partial melting of hydrous mafic compositions. Earth Planet Sci Lett 42: 191–201

Henderson P (1984) General geochemical properties and abundances of the rare earth elements. In: Henderson P (ed) Rare earth element geochemistry. Elsevier, Amsterdam, pp 1–29

Hofmann AW (1988) Chemical differentiation of the earth: the relationship between mantle, continental crust, and oceanic crust. Earth Planet Sci Lett 90: 297–314

Hoxha M (1993) Etude structurale et pétrologique des péridotites de l'ophiolite de Kukes (Albanie): cinématique de la déformation et géométrie de la ride. Thèse d'univ INPL, Nancy

Ionov DA, Savoyant L, Dupuy C (1992) Application of the ICP-MS technique to trace element analysis of peridotites and their minerals. Geostand Newsl 16: 311–315

Ionov DA, Dupuy C, O'Reilly SY, Kopylova MG, Genshaft YS (1993) Carbonated peridotite xenoliths from Spitzbergen: implications for trace element signature of mantle carbonate metasomatism. Earth Planet Sci Lett 119: 283–297

Irving AJ, Frey FA (1984) Trace element abundances in megacrysts and their host basalts: constraints on partition coefficients and megacrysts genesis. Geochim Cosmochim Acta 48: 1201–1221

Jurewicz AJG, Watson EB (1988) Cations in olivine. 2 Contrib Mineral Petrol 99: 186–201

Kempton PD (1987) Mineralogic and geochemical evidence for differing styles of metasomatism in spinel lherzolite xenoliths: enriched mantle source regions of basalts? In: Menzies MA, Hawkesworth CJ (eds) Mantle metasomatism. Academic Press Inc., London, pp 45–89

Le Bas MJ (1989) Nephelinitic and basanitic rocks. J Petrol 30: 1299–1312

Lee D-C, Halliday AN, Davies GR, Essene EJ, Fitton JG, Temdjim R (1996) Melt enrichment of shallow depleted mantle: a detailed petrological, trace element and isotopic study of mantle- derived xenoliths and megacrysts from the Cameroon Line. J Petrol 37: 415–441

Lemarchand F, Villemant B, Calas G (1987) Trace element distribution coefficients in alkaline series. Geochim Cosmochim Acta 51: 1071–1081

Lloyd FE (1987) Characterization of mantle metasomatic fluids in spinel lherzolites and alkali clinopyroxenites from the west Eifel and south west Uganda. In: Menzies MA, Hawkesworth CJ (eds) Mantle metasomatism. Academic Press Inc., London, pp 91–123

Machado N, Brooks C, Hart SR (1986) Determination of initial 87Sr/86Sr and 143Nd/144Nd in primary minerals from mafic and ultramafic rocks: experimental procedure and implications for the isotopic characteristics of the Archean mantle under the Abitibi greenstone belt, Canada. Geochim Cosmochim Acta 50: 2335–2348

Mason PRD, Downes H, Thirlwall MF, Seghedi I, Szakacs A, Lowry D, Mattey D (1996) Crustal assimilation as a major petrogenetic process in the East Carpathian Neogene and Quaternary continental margin arc, Romania. J Petrol 37: 927–959

McInnes BIA, Cameron EM (1994) Carbonated, alkaline hybridizing melts from a sub-arc environment: mantle wedge samples from the Tabar-Lihir-Tanga-Feni arc, Papua New Guinea. Earth Planet Sci Lett 122: 125–141

Meen JK (1987) Mantle metasomatism and carbonatites; an experimental study of a complex relationship. In: Morris EM, Pasteris JD (eds) Mantle metasomatism and alkaline magmatism. Geol Soc Am, Boulder, pp 91–100

Mercier J-C (1985) Olivine and pyroxenes. In: Wenk HR (ed) Preferred orientation in deformed metals and rocks: an introduction to modern texture analysis. Academic Press Inc., New-York, pp 407–430

Mercier J-C, Nicolas A (1975) Textures and fabrics of upper mantle peridotites as illustrated by xenoliths from basalts. J Petrol 16: 454–487

Newton RC (1986) Metamorphic temperatures and pressures of group B and C eclogites. Geol Soc Am Mem 17–30

Nicolas A, Prinzhofer A (1983) Cumulative or residual origin for the transition zone in ophiolites: structural evidence. J Petrol 24: 188–206

Nriagu JO, Moore PB (1984) Phosphate minerals. Springer-Verlag, Berlin Heidelberg New York

Pécskay Z (1995) Petrology and geochemistry of late Tertiary/ Quaternary mafic alkaline volcanism in Romania. Lithos 35: 65–82

Pécskay Z, Lexa J, Szakacs A, Baloh K, Seghedi I, Konecn V, Kovacs M, Marton E, Kaliciak M, Széky-Fux V, Poka T, Gyarmati P, Edelstein O, Rosu E, Zec B (1995) Space and time distribution of Neogene–Quaternary volcanism in the Carpatho-Pannonian region. Acta Vulcanol 7(2): 15–28

Pyle JM, Haggerty SE (1994) Silicate-carbonate liquid immiscibility in upper-mantle eclogites: implications for natrosilicic and carbonatitic melts. Geochim Cosmochim Acta 58: 2997–3011

Rampone E, Piccardo GB, Vannucci R, Bottazzi P, Ottolini L (1993) Subsolidus reactions monitored by trace element partitioning: the spinel- to plagioclase-facies transition in mantle peridotites. Contrib Mineral Petrol 115: 1–17

Riley NG Jr, Kohlstedt LD (1991) Kinetics of melt migration in upper mantle-type rocks. Earth Planet Sci Lett 105: 500–521

Rogers NW, Hawkesworth CJ, Parker RJ, Marsh JS (1985) The geochemistry of potassic lavas from Vulsini, central Italy, and

implications for mantle enrichment processes beneath the Roman region. Contrib Mineral Petrol 90: 244–257

Rudnick RL (1992) Xenoliths – samples of the lower continental crust. In: Fountain DM, Arculus RJ, Kay RW (eds) Continental lower crust. Elsevier, Amsterdam, pp 269–308

Rudnick RL, McDonough WF, Chappell BW (1993) Carbonatite metasomatism in the northern Tanzanian mantle: petrographic and geochemical characteristics. Earth Planet Sci Lett 114: 463–475

Seghedi I, Szakacs A, Mason P (1995) Petrogenesis and magmatic evolution in the East Carpathian Neogene volcanic arc (Romania). Acta Vulcanol 7(2): 135–144

Sharbert HG (1993) The petrogenesis of Pliocene alkaline volcanic rocks from the Pannonian Basin, Eastern Central Europe. J Petrol 34: 317–343

Simonetti A, Bell K (1994) Nd, Pb and Sr isotopic data from the Napak carbonatite-nephelinite centre, eastern Uganda: an example of open-system crystal fractionation. Contrib Mineral Petrol 115: 356–366

Sobolev NV, Shatsky VS (1990) Diamond inclusions in garnets from metamorphic rocks: a new environment for diamond formation. Nature 343: 742–746

Sun S-s (1982) Chemical composition and origin of the Earth's primitive mantle. Geochim Cosmochim Acta 46: 179–192

Urai JL, Means WD, Lister GS (1986) Dynamic recrystallization of minerals. In: Hobbs, BE, Heard HC (eds) Mineral and rock deformation: laboratory studies. Geophys Monogr 36, Washington, USA, pp 161–200

Vanucci R, Piccardo GB, Rivalenti G, Zanetti A, Rampone E, Ottolini L, Oberti R, Mazzucchelli M, Bottazzi P (1995) Origin of LREE-depleted amphiboles in the subcontinental mantle. Geochim Cosmochim Acta 59: 1763–1771

Vaselli O, Downes H, Thirlwall M, Dobosi G, Coradossi N, Seghedi I, Szakacs A, Vannucci R (1995) Ultramafic xenoliths in Plio-Pleistocene alkali basalts from the eastern Transylvanian Basin: depleted mantle enriched by vein metasomatism. J Petrol 36: 23–53

Wass SY, Rogers NW (1980) Mantle metasomatism—precursor to continental alkaline volcanism. Geochim Cosmochim Acta 44: 1811–1823

Watson EB (1982) Melt infiltration and magma evolution. Geology 10: 236–240

Watson EB, Harrison TM (1983) Zircon saturation revisited: temperature and composition effects in a variety of crustal magma types. Earth Planet Sci Lett 64: 295–304

Wenzel F (1997) Tectonics of the Vrancea zone (Romania) (abstract). EUG 9, Terra Nova, Strasbourg 23–27 March 1997, pp 155

Wilson M (1989) Igneous petrogenesis: a global tectonic approach. Unwin Hyman, London

Wilson M, Downes H (1992) Mafic alkaline magmatism associated with the European Cenozoic rift system. Tectonophysics 208: 173–182

Wilson M, Rosenbaum JM, Dunworth EA (1995) Melilitites: partial melts of the thermal boundary layer ? Contrib Mineral Petrol 119: 181–196

Witt G, Seck HA (1989) Origin of amphibole in recrystallised and porphyroclastic mantle xenoliths from the Rhenish Massif: implications for the nature of mantle metasomatism. Earth Planet Sci Lett 91: 327–340

Witt-Eickschen G (1993) Upper mantle xenoliths from alkali basalts of the Vogelsberg, Germany: implications for the mantle upwelling and metasomatism. Eur J Mineral 5: 361–376

Witt-Eickschen G, Seck HA, Reys C (1993) Multiple enrichment processes and their relationships in the subcrustal lithosphere beneath the Eifel (Germany). J Petrol 34, 1: 1–22

Wood BJ, Banno S (1973) Garnet-orthopyroxene and orthopyroxene-clinopyroxene relationships in simple and complex systems. Contrib Mineral Petrol 42: 109–124

Woolley AR, Kempe DRC (1989) Carbonatites: nomenclatures, average chemical compositions, and element distribution. In: Bell K (ed) Carbonatites: genesis and evolution. Unwyn Hyman, London, pp 1–14

Wörner G, Beusen J-M, Duchateau N, Gijbels R, Schmincke H-U (1983) Trace element abundances and mineral/melt distribution coefficients in phonolites from the Laacher See Volcano (Germany). Contrib Mineral Petrol 84: 152–173

Yaxley GM, Crawford AJ, Green DH (1991) Evidence for carbonatite metasomatism in spinel peridotite xenoliths from western Victoria, Australia. Earth Planet Sci Lett 107: 305–317

Zanetti A, Vanucci R, Bottazzi P, Oberti R, Ottolini L (1997) Infiltration metasomatism at Lherz as monitored by systematic ion-microprobe investigations close to a hornblendite vein. Chem Geol (in press)